



# AMERICAN METEOROLOGICAL SOCIETY

*Journal of Climate*

## **EARLY ONLINE RELEASE**

This is a preliminary PDF of the author-produced manuscript that has been peer-reviewed and accepted for publication. Since it is being posted so soon after acceptance, it has not yet been copyedited, formatted, or processed by AMS Publications. This preliminary version of the manuscript may be downloaded, distributed, and cited, but please be aware that there will be visual differences and possibly some content differences between this version and the final published version.

The DOI for this manuscript is doi: 10.1175/2010JCLI3373.1

The final published version of this manuscript will replace the preliminary version at the above DOI once it is available.



1  
2  
3  
4

5 **The NCEP GODAS Ocean Analysis of the Tropical Pacific Mixed Layer Heat**  
6 **Budget on Seasonal to Interannual Time Scales**

7  
8  
9

10

11 Boyin Huang<sup>1\*</sup>, Yan Xue<sup>1</sup>, Dongxiao Zhang<sup>2</sup>, Arun Kumar<sup>1</sup>, and Michael J. McPhaden<sup>2</sup>

12

13

14

15 (First revision for J. Climate. January 20, 2010)

16

17

18

19

20 <sup>1</sup>Climate Prediction Center, NOAA, Maryland

21 <sup>2</sup>Pacific Marine and Environmental Laboratory, NOAA, Washington

---

\* Corresponding author address:

Dr. Boyin Huang, Wyle Information Systems and Climate Prediction Center, NOAA  
605A WWB, 5200 Auth Road, Camp Springs, Maryland. Email. boyin.huang@noaa.gov

1 **Abstract**

2       The mixed layer heat budget in the tropical Pacific is diagnosed using pentad (5  
3 day) averaged outputs from the Global Ocean Data Assimilation System (GODAS),  
4 which is operational at the National Centers for Environmental Prediction (NCEP). The  
5 GODAS is currently used by NCEP's Climate Prediction Center (CPC) to monitor and to  
6 understand El Niño and La Niña in near real-time. The purpose of our study is to assess  
7 the feasibility of using an operational ocean data assimilation system to understand SST  
8 variability.

9       The climatological mean and seasonal cycle of mixed layer heat budgets derived  
10 from GODAS agree reasonably well with previous observational and model based  
11 estimates. However, significant differences and biases were noticed. Large biases were  
12 found in GODAS zonal and meridional currents, which contributed to biases in the  
13 annual cycle of zonal and meridional advective heat fluxes. The warming due to tropical  
14 instability waves in boreal fall is severely underestimated due to use of 4-week data  
15 assimilation window. On interannual time scales, the GODAS heat budget closure is  
16 good for weak-to-moderate El Niños. A composite for weak-to-moderate El Niños  
17 suggests that zonal and meridional temperature advection and vertical  
18 entrainment/diffusion all contributed to the onset of the event, and that zonal advection  
19 played the dominant role during the decay of the event and the transition to La Niña. The  
20 net surface heat flux acts as a damping during the development stage, but plays a critical  
21 role in the decay of El Niño and the transition to the following La Niña.

22       The GODAS heat budget closure is generally poor for strong La Niñas. Despite  
23 the biases, the GODAS heat budget analysis tool is useful in monitoring and  
24 understanding the physical processes controlling the SST variability associated with  
25 ENSO. Therefore it has been implemented operationally at CPC in support of NOAA's  
26 operational ENSO forecasting.

## 1 **1. Introduction**

2           Understanding changes in sea surface temperature (SST) is key to understanding  
3 the coupled atmosphere-ocean system. For example, for better understanding and ability  
4 to forecast El Niño-Southern Oscillation (ENSO), which is the dominant mode of  
5 coupled ocean-atmospheric variability in the tropical Pacific, many studies have analyzed  
6 the physical mechanisms that govern the seasonal cycle and interannual variability of  
7 SST (Stevenson and Niiler 1983; Hayes et al. 1991; Chen et al. 1994; Kessler et al. 1998;  
8 Wang and McPhaden 1999, 2000, and 2001a; Swenson and Hansen 1999; Vialard et al.  
9 2001; Kim et al. 2007).

10           The near surface ocean is forced by winds, downward shortwave and longwave  
11 radiation fluxes, and fresh water fluxes. The ocean then impacts the atmosphere via  
12 latent, sensible, and longwave radiative heat losses that are dependent on SST and near-  
13 surface atmospheric variables. Since SST is closely related to mixed layer temperature  
14 variability, SST variations are intimately connected with the heat budget of the mixed  
15 layer. Various approaches, differing in their use of input data, have been taken to analyze  
16 the heat budget of the mixed layer. One approach is the use of observational data.  
17 Because of the scarcity of the observational data, however, such analyses have difficulty  
18 in accurately calculating the necessary horizontal and vertical gradient terms in the heat  
19 budget equations (Hayes et al. 1991; Wang and McPhaden 1999, hereafter WM99).

20           An alternate approach is the use of output from model simulations (Chen et al.  
21 1994; Kessler et al. 1998, hereafter KRC98; Vialard et al. 2001; Zhang et al. 2007; Zhang  
22 2008, hereafter ZH08). Although the analysis based on model simulations can precisely  
23 calculate various terms in the budget equations, such analyses can deviate substantially  
24 from observed reality because of the uncertainty in atmospheric forcing and other model

1 biases. Further, because of nonlinearities, heat budgets may close when data from daily  
2 model outputs are analyzed, but may not when only monthly outputs from the model  
3 simulations are available (Zhang et al. 2007). A third approach is the use of output from  
4 an ocean data assimilation system (Kim et al. 2007). A particular advantage of using  
5 ocean assimilation products is that the model solutions are partially constrained by  
6 observations so that departures from the observations, unlike for the model simulations,  
7 may not be as large.

8         Kim et al. (2007) used the data assimilation product called Estimating the  
9 Circulation and Climate of the Ocean (ECCO; <http://www.ecco-group.org>) to analyze the  
10 mixed layer temperature variability in the NINO3 region. ECCO is an adjoint-based  
11 estimation system that demands the estimated state satisfies the model equations exactly  
12 over a certain time interval while adjusting control variables, which are typically the  
13 initial state, surface forcing, and model parameters, so that the estimated states are as  
14 close to observations as possible. Kim et al. (2007) suggested that such systems ensure  
15 consistency of the estimated surface forcing with the estimated ocean state, thus  
16 guaranteeing the closure of heat budgets.

17         In this study, we use the pentad (five-day) averaged outputs from the Global  
18 Ocean Data Assimilation System (GODAS) (Behringer et al. 1998; Behringer and Xue  
19 2004) produced at National Centers for Environmental Prediction (NCEP). GODAS is a  
20 sequential estimation system that allows the estimated state to deviate from an exact  
21 solution of the underlying physical model by applying statistical corrections to the state.  
22 These corrections often make estimated states close to observations, but they imply  
23 internal sources and sinks of heat, salt, and momentum, etc. Therefore, the heat budgets  
24 derived from GODAS will not have a perfect closure as that in Kim et al. (2007).

1 However, we will show that the heat budget derived from GODAS is approximately  
2 closed on seasonal to interannual time scales. In particular, this budget is useful in  
3 understanding and monitoring the physical processes controlling the SST variability  
4 associated with ENSO.

5 Previous model and observational studies have suggested that the mechanisms for  
6 mixed layer temperature variability are very complicated. For example, for the seasonal  
7 cycle, the net surface heat flux, subsurface entrainment/diffusion cooling, and tropical  
8 instability waves (TIW) all play an important role (KRC98, WM99, Philander et al. 1986;  
9 Contreras 2002; Jochum and Murtugudde 2006). For the eastern Pacific on interannual  
10 time-scales, vertical entrainment/diffusion is the most critical process controlling  
11 interannual SST variability (Harrison et al. 1990; Frankignoul et al. 1996; Wang and  
12 McPhaden, 2000, 2001a; Zhang et al. 2007; Kim et al. 2007), while the surface heat  
13 fluxes act to damp interannual SST variations. For the central and western equatorial  
14 Pacific, studies have suggested that zonal advection by anomalous currents is the  
15 dominant mechanism for SST variation on interannual timescales (Kessler and McPhaden  
16 1995).

17 For a heat budget analysis based on the output of an ocean data assimilation  
18 system, the question remains about how well earlier conclusions can be replicated and  
19 what new can be learned. In this study, we use the pentad (five-day) averaged outputs  
20 from GODAS to diagnose heat budgets of the mixed layer in the tropical Pacific. The  
21 GODAS outputs have been extensively used at Climate Prediction Center (CPC) of  
22 NCEP to monitor global ocean variability and its interaction with the atmosphere (see  
23 CPC's Monthly Ocean Briefing archive at  
24 <http://www.cpc.ncep.noaa.gov/products/GODAS>). An advantage of using GODAS

1 outputs for the mixed layer heat budget analysis is that, if realistic, it can be routinely  
2 updated in real-time to monitor the mixed layer heat budget and to understand the sources  
3 of SST variability (particularly on ENSO time scales) in the tropical Pacific.

4 The purpose, and a unique aspect, of the paper is to demonstrate the feasibility of  
5 an ocean data assimilation product, i.e., GODAS, for the analysis of the evolution of the  
6 mixed layer in the tropical Pacific. We will discuss the realistic and potentially  
7 problematic features of the analysis for the annual mean and seasonal cycle, as well as for  
8 interannual variability of the mixed layer temperature in the tropical Pacific. Based on the  
9 results and comparison with earlier studies, we demonstrate that the analysis of the mixed  
10 layer heat budget from an operational ocean assimilation system is an effective tool to  
11 monitor and understand SST variability on ENSO time scales. Special attention will be  
12 given to the issue of heat budget closure when the dynamical consistency of model  
13 solutions is not maintained due to the ingestion of data in the assimilation cycle.

14 We briefly describe the NCEP operational GODAS in Section 2, and data and  
15 validation procedures in Section 3. The methodology for the mixed layer heat budget  
16 calculations is discussed in Section 4. Mixed layer heat budget governing the mean,  
17 seasonal cycle, and composite El Niño is presented in Section 5.

## 18 19 **2. A Description of the NCEP GODAS**

20 GODAS was implemented at NECP in 2004 (Behringer and Xue 2004) and is  
21 currently used to initialize the oceanic component of NCEP's Climate Forecast System  
22 (Saha et al. 2007). It replaced the Pacific Ocean Data Assimilation System (ODAS)  
23 version RA6 (Ji et al. 1995; Behringer et al. 1998). The major changes from the RA6  
24 included 1) an extension to a quasi-global domain (75°S-65°N), 2) a replacement of the

1 Geophysical Fluid Dynamics Laboratory's Modular Ocean Model (MOM) version 1 with  
2 version 3 (Pacanowski and Griffies 1999), 3) a change from momentum flux forcing only  
3 to momentum, heat, and fresh water flux forcings from the NCEP Reanalysis 2 (or R2)  
4 (Kanamitsu et al. 2002), and, 4) a change in the assimilation from temperature only to  
5 temperature and synthetic salinity that is constructed from temperature and a local  
6 temperature/ salinity climatology.

7         The ocean model has a resolution of  $1^\circ$  by  $1^\circ$  that increases to  $1/3^\circ$  in the N-S  
8 direction within  $10^\circ$  of the equator, and has 40 levels with a 10 meter resolution in the  
9 upper 200 meters. Other features of MOM3 include an explicit free surface, the Gent-  
10 McWilliams isoneutral mixing scheme (Gent and McWilliams 1990), and the K-profile  
11 parameterization (KPP) vertical mixing scheme (Large et al. 1994).

12         Temperature observations assimilated into GODAS include data from expendable  
13 bathythermographs (XBTs), Tropical Atmosphere Ocean (TAO) array in the tropical  
14 Pacific, Triangle Trans Ocean Buoy Network (TRITON) in the tropical Indian Ocean,  
15 Prediction and Research Moored Array in the Tropical Atlantic (PIRATA), and Argo  
16 profiling floats (see references cited in Huang et al. 2008). In the assimilation cycle, the  
17 model state is corrected by observations within 4 week window centered on the model  
18 time using a 3DVAR scheme (Behringer et al. 1998). The 4 week assimilation window is  
19 effective in eliminating unrealistic small scale variations and improving large scale  
20 structures, but it severely smoothes out variations associated with Tropical Instability  
21 Wave (TIW). Due to the lack of direct salinity observations, synthetic salinity profiles  
22 constructed from temperature and a local T-S climatology are also assimilated into  
23 GODAS. During the assimilation cycle the surface fluxes from R2 are further corrected  
24 by restoring the model temperature of the first layer (5 meter) to the Optimal

1 Interpolation (OI) SST analysis version 2 (Reynolds et al. 2002), and restoring the model  
2 surface salinity to the annual sea surface salinity (SSS) climatology (Conkright et al.  
3 1999). The restoring timescale is 5 days for temperature and 10 days for salinity. The  
4 strong restoration to observed SST is necessary so that the model SST is close to  
5 observations. The heat flux correction due to the SST relaxation is significant and has  
6 been included in our heat budget analysis.

7 GODAS has only pentad and monthly outputs. This study uses the pentad outputs  
8 of temperature, salinity and 3-dimensional ocean currents on a common  $1^{\circ}\times 1^{\circ}$  grid in the  
9 1979-2008 period. The choice of pentad fields and  $1^{\circ}\times 1^{\circ}$  grid has little negative impact  
10 on the GODAS heat budget analysis since TIW is severely underestimated in GODAS  
11 due to its use of 4 week data assimilation window.

12

### 13 **3. Data and GODAS Validation**

14 Observed data and analyses are used to validate GODAS, which include monthly  
15 weekly OI SST, climatological salinity and temperature from the World Ocean Database  
16 2001 (WOD01) (Conkright et al. 2002); pentad currents from Ocean Surface Current  
17 Analysis-Real Time (OSCAR) (Bonjean and Lagerloef 2002); daily temperature, salinity,  
18 and currents from TAO moorings (<http://www.pmel.noaa.gov/tao>); surface heat fluxes  
19 from Objectively Analyzed air-sea Fluxes (OAFlux) (Yu and Weller 2008); and solar and  
20 longwave radiation heat fluxes from International Satellite Cloud Climatology Project  
21 (ISCCP, <http://isccp.giss.nasa.gov>). Earlier validation of GODAS suggested that the  
22 temperature field is closer to observations than the Pacific ODAS and that the poor  
23 salinity field in ODAS is dramatically improved (Behringer and Xue 2004). Although  
24 this version of GODAS does not assimilate satellite altimetry, the sea surface height in

1 GODAS is also reasonably consistent with altimetry and tide gauge records (Behringer  
2 and Xue 2004; Behringer 2007).

3 Before analyzing the mixed layer heat budget, we first quantify the accuracy of  
4 GODAS in representing the mixed layer temperature and ocean currents. The seasonal  
5 cycle of temperature along the equator is well simulated by GODAS and differences from  
6 the observed seasonal cycle are generally less than 0.5°C (not shown). Zonal current  
7 along the equator (1°S-1°N) is compared with OSCAR (Fig. 1). The OSCAR currents  
8 (Fig. 1a) are based on an analysis of satellite altimeter and scatterometer measurements,  
9 and the seasonal cycle is based on the 1993-2007 analysis period  
10 (<http://www.oscar.noaa.gov/index.html>). Compared to OSCAR currents, GODAS has a  
11 westward bias in the far western and eastern equatorial Pacific and an eastward bias in  
12 the central Pacific between 180° and 120°W (Fig. 1c). Biases in the western and central  
13 Pacific are likely associated with the assimilation of synthetic salinity, as these biases are  
14 dramatically reduced in an experimental GODAS assimilation run where observed  
15 salinity from Argo floats is also assimilated (Behringer 2007).

16 Next, GODAS and OSCAR currents are compared with the measurements at four  
17 TAO mooring locations along the equator in the western (165°E), central (170°W), and  
18 eastern (140°W and 110°W) Pacific. Figures 2a-h show the annual cycles of zonal and  
19 meridional currents from GODAS, OSCAR and TAO observations, and Tables 1-2 show  
20 the comparison statistics between OSCAR and TAO, and between GODAS and TAO. In  
21 Tables 1-2, mean bias was calculated as the mean difference between model and TAO  
22 data for the common period of two data sets; root-mean-square-error (RMSE) was  
23 calculated with the total currents; anomaly correlation coefficient (ACC) and anomaly  
24 RMSE (ARMSE) were calculated from currents for which the means have been removed.

1 For zonal currents, OSCAR generally agrees with TAO better than GODAS does.  
2 The mean biases are -18, 13, -4, -2 cm s<sup>-1</sup>, respectively, at 165°E, 170°W, 140°W, and  
3 110°W in OSCAR; and are -24, 23, 13, and -18 cm s<sup>-1</sup> in GODAS (Table 1). The RMSEs  
4 are 19, 14, 8, and 5 cm s<sup>-1</sup>, respectively, at 165°E, 170°W, 140°W, and 110°W in  
5 OSCAR; and are 26, 26, 15, and 18 cm s<sup>-1</sup> in GODAS (Table 1). Interestingly, both  
6 OSCAR and GODAS have reasonably high ACCs (0.93, 0.94, 0.95, and 0.98 in OSCAR;  
7 and 0.76, 0.80, 0.96, and 0.98 in GODAS) with TAO observations. The anomalous  
8 RMSEs (5, 6, 7, 5 cm s<sup>-1</sup> in OSCAR, and 10, 11, 7 and 5 cm s<sup>-1</sup> in GODAS) are much  
9 smaller than RMSEs that include the mean biases. In summary, both GODAS and  
10 OSCAR have large mean biases in zonal currents in the western (165°E) and central  
11 (170°W) Pacific, and GODAS has much larger mean biases than OSCAR does in the  
12 eastern (140°W, and 110°W) Pacific. Once the mean biases are removed, both OSCAR  
13 and GODAS simulate TAO observations reasonably well. It will be shown in Section 5  
14 that GODAS is quite adequate in simulating anomalous zonal advective heat flux in the  
15 central-eastern tropical Pacific associated with ENSO.

16 For meridional currents, the OSCAR estimates are generally too weak and bear  
17 little resemblance to TAO observations (Fig. 2e-h). In contrast, GODAS currents have  
18 amplitudes comparable to those of observations. GODAS meridional currents are  
19 superior to OSCAR meridional currents in the western (165°E) and the central-eastern  
20 (170°W and 140°W) Pacific. The RMSE are 4, 8, 4, and 2 cm s<sup>-1</sup>, respectively, at 165°E,  
21 170°W, 140°W, and 110°W in OSCAR; and 2, 4, 4, 3 cm s<sup>-1</sup> in GODAS (Table 2). The  
22 ACCs are 0.59, 0.90, 0.56, and 0.44 in GODAS; but are near zero in OSCAR except in  
23 the far eastern (110°W) Pacific.

1           It is very interesting that for zonal currents, OSCAR is generally superior to  
2 GODAS in the central and eastern Pacific (170°W, 140°W and 110°W), but they are both  
3 poor in the western Pacific (165°E). An experimental GODAS run suggested that the  
4 large biases in GODAS zonal currents can be significantly reduced when the Argo  
5 salinity is assimilated (Behringer 2007). For the meridional currents, GODAS is  
6 generally superior to OSCAR in the western (165°E) and central-eastern (170°W and  
7 140°W) Pacific, but OSCAR is superior to GODAS in the eastern Pacific (110°W).  
8 However, the amplitude of GODAS meridional currents is more realistic than that of  
9 OSCAR, which is too weak. The smaller RMSE in OSCAR than in GODAS in the  
10 eastern Pacific is probably due to the smaller amplitude in OSCAR.

11

#### 12 **4. Methodology for Analyzing the Mixed Layer Heat Budget**

##### 13 *a. Mixed layer depth*

14           The criterion to calculate mixed layer depth (MLD) is often defined differently  
15 based on requirements of the analysis (You 1995; Sprintall and Tomczak 1992). We  
16 select the criterion to be a density difference of  $0.125 \text{ kg m}^{-3}$  between the surface and the  
17 bottom of the mixed layer. The results of the heat budget analysis, however, are not  
18 sensitive to the choice of the criterion. In fact, similar results were obtained when the  
19 criterion was chosen to be temperature difference of 0.5 K.

20           The MLD of GODAS is calculated using the pentad fields of temperature and  
21 salinity. The seasonal cycle of the GODAS MLD is calculated based on the 1982-2004  
22 period and is compared with the MLD of WOD01 that is calculated using monthly  
23 climatological fields of temperature and salinity in WOD01.

1           The seasonal cycle of MLD along the equator (1°S-1°N) from WOD01 and  
 2   GODAS, and their differences, are shown in Figure 3. The WOD01 MLD is relatively  
 3   shallow (deep) in the western and eastern (central) tropical Pacific (Fig. 3a). The shallow  
 4   MLD in the eastern tropical Pacific is associated with the shallow thermocline maintained  
 5   by easterly trade winds in the central tropical Pacific. The shallow MLD in the western  
 6   tropical Pacific is associated with the excess of precipitation over evaporation that forms  
 7   a barrier layer (Sprintall and Tomczak 1992; Ando and McPhaden 1997). Compared to  
 8   WOA01, the MLD based on GODAS is about 20-30 m too deep in the west-central  
 9   Pacific through the calendar year, and is about 10-20 m too deep in the eastern Pacific  
 10   during boreal fall.

11  
 12   *b. Mixed layer temperature equation*

13           The temperature equation for the mixed layer, described by Stevenson and Niiler  
 14   (1983), is expressed as (see details in Appendix A):

15    $T_t = F$  (1)

16    $F = Q_u + Q_v + Q_w + Q_q + Q_{zz}$  (2)

17   where  $T_t = \frac{\partial T_a}{\partial t}$  is the mixed layer temperature tendency, and F is the combined forcing

18   of zonal advection ( $Q_u$ ), meridional advection ( $Q_v$ ), vertical entrainment ( $Q_w$ ), adjusted

19   surface heat flux ( $Q_q = \frac{Q_{adj}}{\rho c_p h}$ ), and vertical diffusion ( $Q_{zz} = \frac{Q_{diff}}{\rho c_p h}$ ).  $Q_{adj}$  is the net

20   surface heat flux plus heat flux correction minus the penetrative shortwave radiation [see

21   Eq (A4)]. Weak horizontal diffusion was ignored in our analysis.

1 In order to understand the physical processes that control the temperature  
2 variations in the mixed layer on different time scales, each variable associated with  
3 forcing  $F$  in Eq. (2) is decomposed into low frequency variation ( $\geq 75$  day) and high  
4 frequency transients (hereafter referred to as eddy). Therefore, equation (1) becomes

$$5 \quad T_t = Q_u^L + Q_v^L + Q_w^L + Q_q^L + Q_{zz}^L + E \quad (3)$$

6 where superscript  $L$  indicates the term calculated using low-pass filtered variables and  $E$   
7 represents the combined terms from high frequency eddies (see details in Appendix B).  
8 Eq. (3) is further decomposed into climatology ( $\bar{\phantom{x}}$ ) and its anomaly ( $\prime$ ). The  
9 equation for anomalous temperature is, by omitting superscript  $L$ ,

$$10 \quad T_t' = Q_u' + Q_v' + Q_q' + Q_w' + Q_{zz}' + E' \quad (4)$$

11 Details about each term in Eq. (4) are described in Appendix B. The climatological mean  
12 and annual cycle of each term in Eq. (3) will be discussed in Sections 5b and 5c. The  
13 anomalous heat budgets described by Eq. (4) will be used to construct a composite El  
14 Niño heat budget, and the characteristics of the anomalous heat budgets for a typical El  
15 Niño will be discussed in Section 5d.

16 A cutoff period of 75 days is chosen to separate seasonal and longer time scale  
17 variability from that associated with TIW, which exhibits a typical periods of 20-30 days  
18 (Jochum and Murtugudde 2006). The annual climatology of the heat budgets did not  
19 change much when different cutoff periods between 30 and 90 days were selected (as  
20 also indicated by KRC1998). This suggests that 60-90 day period oceanic Kelvin waves,  
21 forced by the atmospheric Madden-Julian Oscillation (MJO) and westerly wind bursts, do  
22 not make significant contributions to the climatological heat budgets. However, the  
23 cumulative effects of a sequence of oceanic Kelvin waves make a significant contribution

1 to the anomalous heat budget on seasonal time scales, and are believed to influence the  
2 onset and determination of El Niño (Seo and Xue, 2005). In this paper, we will describe  
3 the heat budget using El Niño composite, which tend to smear out the contributions of  
4 oceanic Kelvin waves that may be of importance in the analysis of specific El Niño  
5 events. The topic of how a sequence of oceanic Kelvin waves contribute to the  
6 anomalous heat budget on seasonal time scales during a specific El Niño event will be  
7 explored in a separate paper.

8

9 *c. Closure of the temperature equation*

10 To test the procedures used for computing mixed layer budgets, we first apply the  
11 proposed methodology to a control simulation (referred to as CNTRL hereafter) that is  
12 identical to GODAS except no observations are assimilated. The pentad fields from  
13 CNTRL are used in the calculation of all heat budget terms in Eq. (1). The pentad  
14 climatology is calculated for 1982-2004, and pentad anomalies are obtained by removing  
15 the pentad climatology from each heat budget term. The closure of the heat budgets is  
16 measured by the consistency between  $T_t$  and  $F$  of Eq. (1). Figures 4a-b show the time  
17 evolution of the  $T_t$  and  $F$  for the annual cycle and interannual variability in the NINO3.4  
18 region ( $5^{\circ}\text{S}$ - $5^{\circ}\text{N}$ ,  $120^{\circ}\text{W}$ - $170^{\circ}\text{W}$ ) during 1979-2007 in the CNTRL run. For both the  
19 annual cycle and the interannual variability there is a close resemblance in the tendency  
20 and forcing term. Temporal correlations between  $T_t$  and  $F$  are above 0.95, and the  
21 RMSEs are less than  $0.09^{\circ}\text{C mon}^{-1}$ . However, in the annual cycle  $F$  is about  $0.1^{\circ}\text{C}$   
22  $\text{mon}^{-1}$  cooler than  $T_t$  from June to December. The cold bias may be related to the  
23 underestimation of the eddy warming in CNTRL during summer/fall. In fact, the annual  
24 mean eddy warming averaged in the region  $0^{\circ}$ - $4^{\circ}\text{N}$  and  $90^{\circ}$ - $140^{\circ}\text{W}$  in CNTRL is  $0.5^{\circ}\text{C}$

1  $\text{mon}^{-1}$ , which is significantly weaker than  $0.8^\circ \text{C mon}^{-1}$  derived in the model study by  
2 Richards et al. (2009). The underestimation of the eddy warming might be due to the use  
3 of 5-day averaged fields and the  $1^\circ$  by  $1^\circ$  degree grid. The results nonetheless suggest  
4 that the temperature equation and its closure are approximately satisfied.

5        Figures 4c-d shows the seasonal cycle and interannual variability of  $T_t$  and F for  
6 GODAS. Data assimilation is expected to introduce sources and sinks of heat and  
7 generate inconsistency between the forcing fields and the analyzed ocean states that will  
8 negatively impact the closure of the mixed layer heat budget. However, the mean  
9 seasonal cycle of  $T_t$  and F follow each other closely, suggesting that the heat sources and  
10 sinks due to data assimilation have only minor impact on the climatological heat budget.  
11 For the seasonal cycle, the anomalous correlation coefficient (ACC) and RMSE between  
12  $T_t$  and F are 0.97 and 0.06, very similar to those for CNTRL. The influence of data  
13 assimilation on the heat budget is more evident in the evolution of  $T_t$  and F anomalies,  
14 with ACC (RMSE) of 0.70 (0.23), which is smaller (larger) than those for CNTRL. Note  
15 that a few factors contribute to the imbalance between  $T_t$  and F, including sources and  
16 sinks of heat due to data assimilation, and uncertainties in the parameterization of vertical  
17 entrainment and vertical diffusion and the use of pentad fields and  $1^\circ \times 1^\circ$  grid. Therefore,  
18 we should not be surprised when  $T_t$  and F are out of balance as evident during the strong  
19 El Niño events (82-83 and 97-98, Fig. 4d). We will make a composite heat budget for  
20 those weak-to-moderate El Niño events where the closure is reasonably good, and then  
21 analyze the heat budget during the strong El Niño events separately where the closure is  
22 poor. We will also diagnose errors in the heat budget through comparison with other  
23 observational and model heat budget analyses.

24

## 1 **5. Analysis of the Mixed Layer Heat Budget**

### 2 *a. Surface heat fluxes*

3           The net surface heat flux plays a critical role in forcing temperature changes in the  
4 mixed layer in the equatorial Pacific. The net surface heat flux forcings used in GODAS  
5 is specified from the NCEP R2 reanalysis, and the climatology of various components  
6 averaged in 1982-2004 is shown in Figures 5a-d. Also shown are the climatologies of  
7 penetrative shortwave radiation (Fig. 5e), the surface heat flux correction (Fig. 5f) due to  
8 the SST relaxation in GODAS, and the adjusted net surface heat flux (Fig. 5g), which is  
9 the net surface heat flux plus flux correction minus penetrative shortwave radiation.

10           Shortwave radiation exhibits a clear semiannual cycle along the equatorial Pacific  
11 as the sun crosses the Equator twice a year (Fig. 5a). It has two maxima near the Dateline  
12 with amplitude of  $240 \text{ W m}^{-2}$  in October and  $200 \text{ W m}^{-2}$  in April. The latent heat flux  
13 also has a semiannual cycle with two maxima of  $140 \text{ W m}^{-2}$  in boreal winter and fall. A  
14 minimum of about  $100 \text{ W m}^{-2}$  occurs in spring in the west-central tropical Pacific (Fig.  
15 5d). The longwave radiation represents a net heat loss from the ocean to the atmosphere  
16 with average amplitude of  $50 \text{ W m}^{-2}$  (Fig. 5b). The sensible heat flux is generally less  
17 than  $5 \text{ W m}^{-2}$  (Fig. 5c). The seasonality in longwave and sensible heat flux is also small.

18           Penetrative shortwave radiation has a semiannual cycle with two maxima of about  
19  $40 \text{ W m}^{-2}$  in boreal spring and fall in the far eastern tropical Pacific where the MLD is  
20 shallow (Fig. 5e). The heat flux correction due to SST relaxation is positive with a  
21 maximum of about  $30 \text{ W m}^{-2}$  in the eastern tropical Pacific in early spring (Fig. 5f)  
22 when the model cold bias is the largest (not shown). Because of the semiannual cycle in  
23 the shortwave radiation and latent heat fluxes, the adjusted net heat flux also has a clear  
24 semiannual cycle with two maxima in boreal spring and late fall in the central and eastern

1 tropical Pacific (Fig. 5g). The analysis indicates that the longwave radiation, penetrative  
2 shortwave radiation, and heat flux corrections all make significant contributions to the  
3 closure of the heat budget, although their magnitudes are relatively small compared with  
4 shortwave radiation and latent heat fluxes.

5 The latent and sensible heat fluxes shown in Figure 5 are similar to the OAFlux,  
6 and differences are generally less than  $10 \text{ W m}^{-2}$  (not shown). Compared with the net  
7 surface heat flux derived from the combination of ISCCP (shortwave and longwave) and  
8 OAFlux (latent and sensible) products, the net surface heat flux from R2 is 40-60  $\text{W}$   
9  $\text{m}^{-2}$  too low in the equatorial Pacific (Fig. 5h), largely due to deficiencies in shortwave  
10 radiation. Shortwave radiation is 40-60  $\text{W m}^{-2}$  too low in boreal spring compared to  
11 ISCCP and WM99. Satellite data from ISCCP suggests that mean shortwave radiation is  
12 as large as 280  $\text{W m}^{-2}$  in boreal fall and 260  $\text{W m}^{-2}$  in early boreal spring in the central  
13 equatorial Pacific (see <http://oaflux.who.edu>).

14 To constrain the drift in surface temperature, GODAS includes a surface heat flux  
15 correction by relaxing model SST to observed SST. The mean flux correction is about  
16 10-30  $\text{W m}^{-2}$  (Fig. 5f). This correction partially compensates for biases in the net surface  
17 heat flux that, if not corrected, would lead to a cooling of upper ocean temperature during  
18 the assimilation cycle. However, the correction is not enough to compensate for all the  
19 deficiencies in the R2 net surface heat flux, which explains why GODAS surface  
20 temperature is still about 0.2°-0.4°C cooler than the observed SST (not shown).

21

## 22 *b. Annual mean mixed layer heat budget*

23 Shown in Figure 6 is the annual mean of the mixed layer heat budget that is  
24 calculated with the low-pass filtered GODAS data (Eq. 3). The mixed layer is heated on

1 average by the adjusted surface heat flux ( $Q_q$ ) at a rate of  $0.2\text{-}0.5^\circ\text{C mon}^{-1}$  in the central  
2 and western Pacific, and  $1\text{-}3^\circ\text{C mon}^{-1}$  in the eastern tropical Pacific (Fig. 6d). The  
3 heating is largely balanced by the cooling from meridional advection ( $Q_v$ ) (Fig. 6b),  
4 vertical entrainment ( $Q_w$ ) (Fig. 6c), and vertical diffusion ( $Q_{zz}$ ) (Fig. 6e). The maximum  
5 cooling by meridional advection is centered off the equator with magnitude of  $1^\circ\text{C mon}^{-1}$   
6 near  $2^\circ\text{N}$ , and  $0.5^\circ\text{C mon}^{-1}$  near  $3^\circ\text{S}$  in the eastern tropical Pacific. The cooling from  
7 vertical entrainment ( $Q_w$ ) is  $0.2^\circ\text{C mon}^{-1}$  in the central tropical Pacific and  $1^\circ\text{C mon}^{-1}$   
8 in the far eastern tropical Pacific. The cooling is larger from vertical diffusion than from  
9 vertical entrainment, and the meridional extension is also broader because upwelling is  
10 mainly constrained within a narrow equatorial band. The annual mean zonal advection  
11 ( $Q_u$ ) (Fig. 6a) contributes to a weak cooling ( $0.2^\circ\text{C mon}^{-1}$ ) across much of the tropical  
12 Pacific. TIW heating (Fig. 6f) is approximately  $0.2^\circ\text{C mon}^{-1}$  in the eastern tropical  
13 Pacific east of  $150^\circ\text{W}$ , and is weaker than in CNTRL ( $0.5^\circ\text{C mon}^{-1}$ ), ZH08 ( $0.5^\circ\text{C}$   
14  $\text{mon}^{-1}$ ), Richards et al. (2009) ( $0.8^\circ\text{C mon}^{-1}$ ), and Jochum and Murtugudde (2006) ( $2^\circ\text{C}$   
15  $\text{mon}^{-1}$ ).

16

### 17 *c. Seasonal cycle of the mixed layer heat budget*

#### 18 1) Seasonal cycle in GODAS

19 The seasonal cycle of the mixed layer heat budget in the equatorial Pacific ( $0.5^\circ\text{N}$ ,  
20 which is selected for the purpose of comparison in the following subsection) is next  
21 discussed. The mixed layer temperature tendency has a strong seasonal cycle in the  
22 equatorial eastern Pacific (Fig. 7e). The positive tendency in early boreal spring is largely  
23 due to excess heating by the adjusted net surface heat flux ( $Q_q$ ; Fig. 7d) over cooling by  
24 vertical entrainment and vertical diffusion ( $Q_w+Q_{zz}$ ; Fig. 7c). In contrast, the negative

1 tendency during late boreal spring to summer is due to cooling by  $Q_w+Q_{zz}$  and  $Q_v$   
2 dominating over heating by  $Q_q$ .

3         The heating by  $Q_q$  is dominated by a semiannual cycle (Fig. 7d). It is largest in  
4 the equatorial eastern Pacific with a primary maximum in boreal spring ( $4^\circ\text{C mon}^{-1}$ ) and  
5 a secondary maximum in boreal fall ( $2^\circ\text{C mon}^{-1}$ ). The semiannual variation of the  
6 heating by  $Q_q$  is critically controlled by cloudiness and mixed layer depth as was pointed  
7 out by KRC98. The magnitude of  $Q_q$  is much weaker ( $0.5^\circ\text{C mon}^{-1}$ ) in the central and  
8 western tropical Pacific than in the east, because the MLD is relatively deep in the west.  
9 Heating in the west-central tropical Pacific is dominated by the semiannual signal in  
10 shortwave radiation (Fig. 5a), which largely governs the temperature tendency (Fig. 7e).

11         Cooling by  $Q_w+Q_{zz}$  remains confined to the central and eastern tropical Pacific  
12 where the MLD is shallow and the vertical temperature gradient is the largest. The  
13 cooling has a primary maximum in boreal spring and a secondary maximum in boreal  
14 summer.

15         The contribution of  $Q_u$  is the largest east of  $130^\circ\text{W}$  (Fig. 7a) and is dominated by  
16 the seasonal cycle: cooling from February to June and a heating from July to January.  
17 This cooling exhibits westward propagation with cooling in the central and eastern  
18 Pacific in the fall (Fig. 7a). The cooling from  $Q_v$  is the largest from May to December  
19 when northerly currents are the strongest (Fig. 2h). The seasonal cycle of TIW heating  
20 (Fig. 7f) is about  $0.5^\circ\text{C mon}^{-1}$  east of  $130^\circ\text{W}$  from June to December.

21

22

23

24

1 2) Comparison with other model simulations

2           The seasonal variation of  $Q_q$  in the equatorial Pacific is similar to that in WM99.  
3 The seasonal variation of  $Q_w+Q_{zz}$  is close to that of ZH08. The pattern of TIW heating  
4 is almost the same as in ZH08.

5           A potential bias in GODAS is the zonal advective cooling in the eastern tropical  
6 Pacific in boreal spring (Fig. 7a), which is inconsistent with results reported in earlier  
7 studies. KRC98 and ZH08 suggested that  $Q_u$  is weakly positive east of  $120^\circ\text{W}$  during  
8 boreal spring largely due to the spring reversal of the South Equatorial Current (SEC).  
9 The erroneous cooling by  $Q_u$  in GODAS is associated with errors in the surface zonal  
10 currents in GODAS for which the spring reversal of SEC does not extend as far eastward  
11 as in OSCAR (Fig. 1). The negative  $Q_u$  in GODAS is generated by the westward surface  
12 zonal currents east of  $105^\circ\text{W}$  (Fig. 1b). Compared with the analysis of ZH08, the cooling  
13 in boreal fall and winter is confined too narrowly in the eastern Pacific and is related to  
14 the eastward biases in GODAS surface zonal currents in the region (Figs. 1c and 2a-2d).

15           Cooling from  $Q_v$  in the eastern Pacific appears too strong in GODAS ( $0.5\text{-}3^\circ\text{C}$ ;  
16 Fig. 7b) when compared with that in ZH08 ( $0.5^\circ\text{C}$ ). Considering GODAS mean  
17 meridional currents do not agree well with observations in the eastern Pacific at  $110^\circ\text{W}$   
18 (Table 2) and GODAS mean temperature has cold biases in the region (not shown), the  
19  $Q_v$  climatology is likely problematic in the eastern Pacific. In addition, the TIW heating  
20 in GODAS (Fig. 7f) is only half of ZH08 ( $1^\circ\text{C mon}^{-1}$ ) and CNTRL ( $1^\circ\text{C mon}^{-1}$ ), and  
21 extends westward to only  $125^\circ\text{W}$  compared to  $150^\circ\text{W}$  in ZH08 and CNTRL.

22

23

24

1 3) Comparison with observational analyses

2 We use the observational analysis of WM99 to further validate the heat budgets of  
3 the mixed layer in GODAS. WM99 used observed winds, temperature, and ocean  
4 currents from the TAO moorings at four locations along the equator in the western  
5 (165°E), central (170°W), and eastern (140°W and 110°W) Pacific. Changes in heat  
6 storage, horizontal heat advection, and heat fluxes at the surface in WM99 were  
7 estimated directly from data. In their estimates, vertical heat flux out of the base of the  
8 mixed layer was calculated as residual, and surface heat fluxes were from COADS. The  
9 heat budgets in GODAS are calculated using unfiltered (total) data to facilitate  
10 comparison with WM99.

11 The temperature tendencies in the mixed layer of GODAS at the four TAO sites  
12 are shown in Figure 8a. According to WM99, the temperature at 110°W warms from  
13 September to March and then cools from April to August. This seasonal variation is  
14 replicated by GODAS except the strong cooling tendency in June is underestimated and  
15 the weak warming tendency in November is missing. Because of the westward  
16 propagation of positive climatological SSTs, the peak warming tendency at 110°W,  
17 140°W, 170°W and 165°W subsequently progresses westward from February to April.  
18 This westward propagation of climatological SST is well simulated by GODAS. The  
19 secondary maximum warming at 165°E in boreal fall indicates a semiannual cycle in the  
20 western tropical Pacific (Yuan 2005).

21 Zonal advection,  $Qu$ , generally cools the eastern (110°W) tropical Pacific during  
22 August to February when the SEC is westward and warms it during the spring reversal of  
23 SEC (Fig. 8b). The warming at 110°W in March-June (Fig. 6b in WM99) is simulated as  
24 cooling in GODAS (Fig. 8b), mainly because GODAS underestimates the spring reversal

1 of SEC in the far eastern Pacific. The cooling at 110°W in boreal fall is seriously  
2 overestimated by GODAS due to westward biases in the surface zonal currents (Figs. 1c  
3 and 2d). Relative to 110°W,  $Q_u$  at 140°W and 170°W is much better simulated by  
4 GODAS, and has a good agreement with the observational analysis of WM99. Zonal  
5 advection at 165°E cools throughout the year and is largely consistent with WM99.

6 Meridional advection,  $Q_v$ , at 110°W and 140°W leads to warming along the  
7 equator with maximum amplitude in boreal summer and fall due to active TIW (WM99;  
8 Chen et al. 1994; KRC98). The  $Q_v$  reaches a minimum during early boreal spring when  
9 TIW is inactive (WM99). In GODAS, warming by  $Q_v$  at 110°W and 140°W (Fig. 8c) is  
10 much weaker ( $0.2^{\circ}$ - $0.5^{\circ}\text{C mon}^{-1}$ ) than in WM99 ( $0.5^{\circ}$ - $2^{\circ}\text{C mon}^{-1}$ ) and it has a secondary  
11 maximum warming during boreal spring (Fig. 8c). The weak warming in  $Q_v$  at 110°W  
12 and 140°W is partly due to biases in the mean meridional currents (Figs. 2g-h) and partly  
13 due to weak TIW. Biases in the low frequency meridional currents may be associated  
14 with biases in wind forcing and biases that result from assimilating synthetic salinity  
15 rather than the observed salinity (Huang et al. 2008).

16 Heating by  $Q_q$  (Fig. 8d) is largest in the eastern Pacific due to a shallow MLD  
17 (Figs. 1b) and is dominated by a semiannual cycle at all four sites. The  $Q_q$  in GODAS  
18 agrees well with that in WM99. One noticeable disagreement is that the second maximum  
19 at 110°W during boreal fall is about twice as large as in WM99. The differences may  
20 result from different methods in calculating  $Q_q$ , although the adjusted net heat flux (Fig.  
21 5g) and MLD (Fig. 1b) in GODAS agrees very well with those of WM99. The  
22 climatology of  $Q_q$  in GODAS is calculated with the pentad  $Q_q$  in the period 1982-2004  
23 and therefore retains the nonlinear relationship between adjusted net heat flux and MLD  
24 (equation A9). In contrast, the climatology of  $Q_q$  in WM99 is based on the climatology

1 of adjusted net heat flux divided by the climatology of MLD. It should also be noted that  
2 there is considerable uncertainty in the mean seasonal cycle of net heat flux itself (Wang  
3 and McPhaden, 2001b).

4 The combined cooling by vertical entrainment and vertical diffusion,  $Q_w+Q_{zz}$ ,  
5 (Fig. 8e) is the largest in the eastern Pacific due to the shallow MLD and strong  
6 upwelling in the region. The  $Q_w+Q_{zz}$  generally agree well with those in WM99.  
7 However, cooling at 110°W in April-August is significantly underestimated in GODAS.  
8 The cooling at 140°W is also weaker in GODAS than in WM99. The weaker cooling by  
9 entrainment and vertical diffusion in GODAS may be associated with biases in zonal  
10 wind stress in R2, which is too weak when compared with QuikSCAT observations and  
11 other products (Josey et al. 2002). The treatment of the vertical entrainment and vertical  
12 diffusion as a residual in WM99 may also contribute to the difference between GODAS  
13 and WM99.

14

#### 15 4) Discussion

16 Mitchell and Wallace (1992) suggested that the seasonal cycle of SST and its  
17 westward propagation are driven by a weakened vertical mixing from December to  
18 March due to weakened meridional wind. Xie (1994) further proposed that the weakening  
19 vertical mixing largely result from the coupling of SST, meridional wind, and  
20 evaporation. Kessler et al. (1998) suggested that both the net heat fluxes and vertical  
21 mixing contributed to the warming tendency from late winter to early spring. They also  
22 pointed out that the solar radiation in spring is larger than that in fall due to minimum in  
23 the cloud cover in spring. Wang and McPhaden (1999, WM99 later) suggested that net  
24 surface heat fluxes and residual subsurface fluxes, equivalent to combination of vertical

1 entrainment and vertical diffusion, are two dominant terms, and tend to cancel out each  
2 other during spring. They emphasized a large warming due to TIW during fall/winter,  
3 and correlation between the mean annual cycle of residual subsurface fluxes and zonal  
4 winds, which implied that the subsurface fluxes are the weakest during spring when zonal  
5 winds are weakest. Vialard et al. (2001) suggested the annual cycle of SST in the NINO3  
6 region is largely controlled by net surface heat fluxes.

7         Compared to above results, the annual cycle heat budget in GODAS has several  
8 shortcomings. Firstly, the TIW warming in boreal fall is severely underestimated in  
9 GODAS (Fig. 7f). Secondly, the low-frequency meridional advection ( $Q_v$ ) is too strong  
10 in boreal summer/fall (Fig. 7b). The biases in  $Q_v$  are probably due to too strong cross-  
11 equatorial winds in the Reanalysis 2 during summer/fall (not shown) that are used to  
12 force the MOM3 model. Thirdly, the vertical entrainment and vertical diffusion  
13 ( $Q_w+Q_{zz}$ ) in boreal summer/fall appears too weak compared to that in WM99, Kessler et  
14 al. (1998) and Vialard et al. (2001) (not shown).

15         Despite these shortcomings, GODAS analysis shows that positive temperature  
16 tendency in the tropical eastern Pacific from December to March is associated with  
17 strengthening of heating by the adjusted heat flux, consistent with WM99, Kessler et al.  
18 (1998), and Vialard et al. (2001). This term dominates over the intensification in cooling  
19 by vertical mixing, both of which are associated with a shoaling mixed layer depth from  
20 December to March (Fig. 3b). The shoaling mixed layer depth is also closely related to  
21 surface heat fluxes and surface winds. Therefore, weakening surface winds, strengthening  
22 net surface heat fluxes and shoaling mixed layer depth all contribute to the warming  
23 tendency of SST from December to March.

24

1 *d. El Niño composite of mixed layer heat budget*

2           In the previous section, the annual mean and the seasonal cycle of mixed layer  
3 heat budget based on GODAS pentad output were discussed. Another important feature  
4 of coupled variability in the equatorial tropical Pacific is ENSO. The ENSO phenomenon  
5 (Philander 1990) is the most prominent interannual climate signal, so the ability of  
6 GODAS to capture the variability of the mixed layer heat budget during the ENSO cycle  
7 is assessed next.

8

9 1) El Niño composite

10           As defined by NOAA's official ENSO index, the Oceanic Niño Index (ONI),  
11 there are eight warm episodes from 1979 to the present. They occurred in 1982-83, 1986-  
12 88, 1991-92, 1994-95, 1997-98, 2002-03, 2004-05, and 2006-07. Many studies have  
13 shown that ENSO episodes are phase locked to the seasonal cycle (Chang et al. 1995;  
14 Tziperman et al. 1998; Galanti and Tziperman 2000; McPhaden and Zhang 2009). The  
15 onset of ENSO events generally occurs early in the year and becomes mature late in the  
16 year or early in the next year (Rasmusson and Carpenter 1982) with the exception of the  
17 1986-88 event whose onset and mature phases were different from others.

18           An El Niño composite is constructed using five weak-to-moderate events (1991-  
19 92, 1994-95, 2002-03, 2004-05, and 2006-07). The 1986-87 event was excluded because  
20 of its unique onset and decay phases. The 1982-83 and 1997-98 events are strong events,  
21 in which nonlinear terms are likely very different from those during weak-to-moderate  
22 events (Jin et al. 2003). In addition, the analysis suggests that the closure of the heat  
23 budget during the two events is not as good as during other El Niño events. We therefore  
24 compare the heat budget of the two events with that discussed in literature separately and

1 assess the feasibility of GODAS in simulating the two strongest events in the past 30  
2 years.

3

#### 4 2) Heat budget for the composite El Niño

5 Shown in Figure 9 are the mixed layer heat budgets for the El Niño composite  
6 averaged between 1°S and 1°N in GODAS. The composite El Niño starts in January of  
7 an El Niño (year 0) and ends in a following La Niña (year +1) (Fig. 9h). The analysis  
8 indicates that heating by entrainment and vertical diffusion ( $Q_w+Q_{zz}$ ) (Fig. 9c),  
9 meridional advection ( $Q_v$ ) (Fig. 9b), and zonal advection ( $Q_u$ ) (Fig. 9a) contribute to El  
10 Niño development during year 0: The heating by  $Q_w+Q_{zz}$  and  $Q_v$  is the strongest east of  
11 140°W; and the heating by  $Q_u$  is distributed over most of the tropical Pacific between  
12 160°E and 110°W.  $Q_q$  is mostly opposite to the composite SST anomalies (Fig. 9h) and  
13 strongly acts to damp El Niño in the eastern tropical Pacific in year 0 and early year +1.  
14 TIW heating (Fig. 9e) also acts weakly to damp El Niño development.

15 El Niño transits to La Niña around April of year +1. A moderate cooling ( $-0.5^{\circ}\sim-$   
16  $1^{\circ}\text{C mon}^{-1}$ ) by  $Q_u$  and  $Q_q$  plays a critical role during the period prior to the transition,  
17 while both  $Q_w+Q_{zz}$  and  $Q_v$  still contribute to a heating in the central-eastern Pacific.  
18 Therefore, zonal advection leads the transition from El Niño to La Niña.

19 After the decay of El Niño, cooling by  $Q_w+Q_{zz}$ ,  $Q_v$ , and  $Q_u$  become strong,  
20 leading to La Niña development during the summer/fall of year +1. Strong heating by  $Q_q$   
21 acts again to damp La Niña development later in year +1.

22 The balance between temperature tendency (Fig. 9f) and forcing (Fig. 9g) appears  
23 good in the central-eastern tropical Pacific. But it is worse in the far eastern tropical  
24 Pacific largely due to biases in zonal currents (Fig. 1c) and underestimation of the TIW

1 heating (Fig. 6f), which is anomalously weak (strong) during El Niño (La Niña) events  
2 (Yu and Liu 2003). The underestimation of TIW heating in GODAS largely resulted from  
3 applying a four-week data assimilation window that smoothes out variations shorter than  
4 30 days. The TIW signal is further weakened by using pentad outputs on  $1^{\circ}\times 1^{\circ}$  grid,  
5 which is available for the analysis.

6         The roles of different oceanic processes and surface heat fluxes in the El Niño  
7 composite in GODAS is further discussed for the NINO 3.4 SST index region ( $5^{\circ}\text{S}$ - $5^{\circ}\text{N}$ ,  
8  $120^{\circ}\text{W}$ - $170^{\circ}\text{W}$ ). Figure 10a shows the spatial average of each flux term in the NINO3.4  
9 region. Lee et al. (2004) suggested that spatially integrated local temperature advection  
10 can be dominated by internal processes such as TIW that redistribute heat within the  
11 domain, and they recommended a new boundary flux approach to analyze the mixed  
12 layer heat budget. Kim et al. (2007) further showed that the spatially integrated zonal  
13 advection tendency in the NINO3 region derived from ECCO analysis is anticorrelated  
14 with the change of SST during the 1997-99 El Niño/La Niña cycle, which disagrees with  
15 the common understanding about the role of large-scale advection of the warm-pool  
16 water during El Niño. Ultimately, the two approaches must be consistent with one  
17 another when all terms in the heat balance are accounted for and properly interpreted, so  
18 our preference is to perform the analysis based on the more conventional local balance  
19 approach.

20         In this analysis the advective temperature terms are further decomposed into  
21 various components described in Eqs. (B5)-(B8). It is seen in Figure 10a that the positive  
22 temperature tendency during the spring of year 0 is due to heating from  $Q_w+Q_{zz}$ ,  $Q_v$  and  
23  $Q_u$ . The temperature tendency changes sign from positive to negative at the end of year  
24 0, which coincides with a rapid transition of  $Q_u$  from heating to cooling. It is interesting

1 that  $Q_v$  does not have a transition until 4-5 month later. This suggests that cooling from  
 2  $Q_u$  and  $Q_q$  plays a dominant role during the decay phase of El Niño and transition to the  
 3 following La Niña, consistent with ENSO recharge-discharge theory (Jin 1997). During  
 4 the summer and fall of year +1, cooling from  $Q_v$  and  $Q_u$  all contributes to the transition  
 5 from El Niño to La Niña as well as the development of La Niña. However,  $Q_w+Q_{zz}$  does  
 6 not appear to contribute the development of La Niña in weak-to-moderate events, which  
 7 is not the case for strong events such as in 1997-98 and 1982-83 that will be discussed  
 8 later.

9 The decomposition of  $Q_u$  in Figure 10b shows that the heating by  $Q_u$  during El  
 10 Niño development in year 0 is dominated by  $-u\overline{T'_x}$  (subscript x, y, and z represents a  
 11 partial derivative, hereafter), and the cooling by  $Q_u$  during La Niña development in year  
 12 +1 is also associated with  $-u\overline{T'_x}$ . This suggests an important role of the zonal advection  
 13 of climatological temperature by anomalous zonal currents in El Niño and La Niña  
 14 development. Note that  $-\overline{uT'_x}$  acts to weakly damp El Niño and TIW acts to weakly  
 15 damp both El Niño and La Niña. For meridional advection, the heating (cooling) by  $Q_v$   
 16 (Fig. 10c) during the development of El Niño in year 0 (La Niña in year +1) in GODAS  
 17 results from both  $-\overline{vT'_y}$  and  $-\overline{v\overline{T'_y}}$  that have comparable amplitude.

18 The decomposition of  $Q_w+Q_{zz}$  in Figure 10d shows that both  $-\overline{wT'_z}$  and  $-w\overline{T'_z}$   
 19 contribute to the development of El Niño and their amplitudes are comparable. During  
 20 the onset phase of El Niño, both  $-w\overline{T'_z}$  and  $-\overline{wT'_z}$  are important, suggesting the role of  
 21 upwelling anomalies ( $-w\overline{T'_z}$ ) is as important as subsurface temperature anomalies  
 22 ( $-\overline{wT'_z}$ ) when El Niño is beginning to develop. During the decay phase of El Niño and  
 23 development phase of La Niña, all components in  $Q_w+Q_{zz}$  act as a weak warming (Fig.

1 10d), which is quite different from those during the strong events of 1997-98 and 1982-  
2 83.

3

### 4 3) Discussion

5         Based on GODAS, the onset phase of El Niño can be attributed to the heating by  
6  $Q_u$ ,  $Q_v$ , and  $Q_w+Q_{zz}$ , which is largely consistent with observational analysis in Wang  
7 and McPhaden (2000). Since  $Q_u$  is dominated by  $-u'\overline{T}_x$  in GODAS (Fig. 10b),  
8 anomalous zonal currents acting on the large climatological SST gradient near the eastern  
9 edge of the warm pool plays a critical role during the onset phase of El Niño, a feature  
10 also noted in previous observational studies (Frankignoul et al. 1996; Picaut et al. 1996;  
11 Wang and McPhaden 2000). The results based on a coupled model simulation also  
12 suggested the importance of  $Q_u$  in El Niño development (Zhang et al. 2007).

13          $Q_v$  contributes to the development of El Niño east of 140°W in GODAS (Fig. 9b).  
14 The decomposition of  $Q_v$  indicates that both  $-\overline{v}T'_y$  and  $-v'\overline{T}_y$  make important  
15 contributions to El Niño development in GODAS, while coupled model simulation  
16 (Zhang et al 2007) suggested that  $-v'\overline{T}_y$  is not as important as  $-\overline{v}T'_y$ . Wang and  
17 McPhaden argued that  $Q_v$  is a damping since TIW dominates this term on the equator  
18 and it generally acts as a damping to SST as indicated in model simulations (Yu and Liu  
19 2003; ZH08; An 2008). This is also true in our analysis of GODAS in the equatorial  
20 Pacific (Figs. 10b-c), but the TIW term is underestimated by GODAS (Fig. 8c).

21         The decomposition of  $Q_w+Q_{zz}$  (Fig. 10d) shows that both  $\overline{w}T'_z$  and  $w'\overline{T}_z$   
22 contribute to the onset phase of El Niño in GODAS. This suggests that both  $w'$  and  
23 subsurface temperature anomalies ( $T'$ ) are key variables to determine El Niño onset, and  
24 is consistent with other observational studies (Wang and McPhaden 2000 and 2001a;

1 Zhang and McPhaden 2006 and 2008). The separation of  $Q_w+Q_{zz}$  (not shown) indicates  
2 that  $Q_{zz}$  plays an important role in the heat budget of the El Niño composite in GODAS.  
3 The observational analyses of 1987-88 (Hayes et al. 1991) and 1991-93 (Kessler and  
4 McPhaden 1995) El Niño events, model analysis of the 1997-98 event (Kim et al. 2007),  
5 and a coupled model simulation (Zhang et al. 2007) all suggested the important role of  
6  $Q_{zz}$ .

7         During the decay phase of El Niño, both  $Q_u$  and  $Q_q$  play a leading role in  
8 GODAS. In fact,  $Q_u$  leads  $Q_v$  by 4-5 months (Fig. 10a).  $Q_u$  is dominated by  $u\overline{T}_x$ , which  
9 suggests that anomalous zonal currents are a precursor for the transition from El Niño to  
10 La Niña. These results are very consistent with previous studies based on observations  
11 (Wang and McPhaden 2000 and 2001a; Vialard et al. 2001) and with coupled model  
12 simulations (An and Jin 2001; Zhang et al. 2007). Observational studies of Wang and  
13 McPhaden (2000 and 2001a) suggested that  $Q_q$  acts as a damping to El Niño because of  
14 the out-of-phase relationship between SST and  $Q_q$ . This damping is particularly  
15 important during the decay phase of El Niño (Figs. 10a and 9d).

16         The  $Q_q$  anomaly is largely due to latent heat flux (Fig. 11a) and its dependence on  
17 anomalies of SST and other near-surface atmospheric variables. Short wave radiation  
18 contributes secondarily to cooling during the peak phase of El Niño. Penetrative solar  
19 radiation,  $Q_{pen}$ , contributes to heating (cooling) when mixed layer depth is anomalously  
20 deep (shallow). Long wave radiation and sensible heat flux  $Q_{long}+Q_{sh}$  are generally  
21 weak. The flux correction,  $Q_{corr}$ , resulting from relaxation to observed SST is relatively  
22 large during the development phase of El Niño and La Niña, indicating biases in surface  
23 heat fluxes and errors in the model physics.

1 For the two strong events of 1997-98 and 1982-83, the mixed layer heat budget  
2 closure is generally poor (Fig. 2d). We pointed out early that the imbalance between  $F$   
3 and  $T_i$  may result from multiple factors including sources and sinks of heat due to data  
4 assimilation, and estimation of vertical diffusion. It should also be noted that the  
5 evolution of mixed layer heat budget during strong El Niño events may differ  
6 significantly from that for weak-to-moderate El Niño events.

7 Next we assess if it is feasible for GODAS to simulate the mixed layer heat  
8 budget of the 1997-98 and 1982-83 events, which are the biggest of the past 30 years.  
9 Figure 12a shows the GODAS budget at 110°W and 0°N from 1997 to 1998. It is clear  
10 that the development of the El Niño in 1997 is largely associated with the anomalous  
11 heating by subsurface ( $Q_w+Q_{zz}$ ) and zonal advection ( $Q_u$ ). The transition from the El  
12 Niño to La Niña results from the anomalous cooling by  $Q_u$  and net surface heat flux  
13 ( $Q_q$ ). The development of La Niña in 1998 is largely associated with the anomalous  
14 cooling by  $Q_w+Q_{zz}$  and  $Q_u$ . These features are largely consistent with the heat budget  
15 composite for weak-to-moderate events (Figure 10a). Differences are that anomalous  
16 cooling by  $Q_w+Q_{zz}$  played the dominant role in the development of the La Niña in 1998,  
17 while  $Q_w+Q_{zz}$  acts as a weak damping in the composite. Meridional advection ( $Q_v$ ) did  
18 not contribute much to the development of the El Niño and acted as a damping to the  
19 development of the La Niña in 1998. However,  $Q_v$  contributed significantly to the  
20 development of the composite El Niño and La Niña (Fig. 10a). The roles of  $Q_w+Q_{zz}$  and  
21  $Q_q$  in our analysis are consistent with the observational analysis of Wang and McPhaden  
22 (2001a; their Figure 6). However, the magnitude of  $Q_w+Q_{zz}$  and  $Q_q$  appears to be  
23 underestimated in our analysis. Some differences were also found in  $Q_u$  and  $Q_v$  between  
24 GODAS and observations.  $Q_u$  contributed to the development of the El Niño in GODAS

1 in 1997, which is consistent with observations. However, it contributed significantly to  
2 the development of the La Niña in GODAS in 1998 instead being a weak damping as in  
3 the observations. Further analysis showed that the anomalous cooling by  $Q_v$  in GODAS  
4 in 1998 is largely associated with  $-u'\overline{T}_x$  (Fig. 12b) because of westward biases in zonal  
5 current anomalies (Fig. 12d).  $Q_v$  contributed moderately to the development of El Niño  
6 in 1997 in the observation, but it was negligible in GODAS (Figs. 12a and 12c). TIW acts  
7 as a weak damping to the El Niño in 1997 and La Niña in 1998 (Figs. 12b and 12c).  
8 Differences at the other three TAO mooring sites (140°W, 170°W and 165°E) are also  
9 large (not shown).

10 For the 1982-83 event (Fig. 13a), anomalous heating and cooling by  $Q_w+Q_{zz}$   
11 played a dominant role in the developments of the El Niño and La Niña in GODAS,  
12 which is very consistent with the observational analysis of Wang and McPhaden (2000a;  
13 their Fig. 5), although the magnitude of these terms was weaker in GODAS than in  
14 observations. Anomalous cooling by  $Q_q$  damped the El Niño in 1982, which are  
15 consistent with observations. Anomalous heating by  $Q_u$  contributed to the development  
16 of the El Niño in GODAS in 1982, which is also consistent with observations, but it  
17 became too strong in 1983 compared with the observations. This is largely due to the  
18 non-linear heating (mainly  $-u'T'_x$ ) (Fig. 13b) that appears to be associated with strong  
19 westward biases of zonal current in GODAS (Fig. 13d). In observations, anomalous  
20 cooling by  $Q_v$  damped the development of the El Niño in 1982 but contributed to the  
21 development of the La Niña in 1983. However, in GODAS  $Q_v$  is very weak in 1982, and  
22 is a moderate damping to the development of the La Niña in 1983 because of heating  
23 from  $-v'\overline{T}_y$  and the non-linear term (Fig. 13c). The TIW acts as a weak damping to the  
24 El Niño in 1982 and La Niña in 1983 (Figs. 13b and 13c).

1           The above results suggest that GODAS simulates  $Q_q$  and  $Q_w+Q_{zz}$  reasonably  
2 well, but contain large biases in  $Q_u$  and  $Q_v$ , most of which are due to biases in surface  
3 currents. It is found that surface current analysis near the equator can be significantly  
4 improved when observed salinity is assimilated into GODAS and the balance between  
5 density and current is properly maintained in the analysis cycle (Behringer 2007).  
6 Therefore, we hope that biases in  $Q_u$  and  $Q_v$  will be significantly reduced in the next  
7 version of GODAS in which the Argo salinity will be assimilated.

## 9 **6. Summary and Discussion**

10           The focus of this paper is to assess the adequacy of GODAS pentad data to  
11 provide a consistent picture of mixed layer heat budget in the tropical Pacific from 1979  
12 to present. We have demonstrated that the mean mixed layer depth was reasonably well  
13 simulated by GODAS east of the dateline, but it was about 10-20 m too deep in the  
14 western Pacific, probably because the water in the western Pacific warm pool was too  
15 salty (Behringer 2007).

16           The climatological mean and seasonal cycle of mixed layer heat budgets derived  
17 from GODAS agree reasonably well with previous observational (WM99) and model  
18 based estimates (KRC96; Vialard et al. 2001). However, significant differences and  
19 biases were noticed. The net surface heat fluxes into the ocean derived from the NCEP  
20 Reanalysis 2 and used to force GODAS are about  $40-60 \text{ W m}^{-2}$  too low in the eastern  
21 equatorial Pacific during boreal spring (Fig. 5h). Large biases were also found in  
22 GODAS zonal and meridional currents (Table 1-2), which contributed to biases in the  
23 annual cycle of zonal and meridional advective heat fluxes,  $Q_u$  and  $Q_v$  (Figs. 7a-b).  
24 However, the interannual variability of the mixed layer heat budget has been simulated

1 reasonably well by GODAS. This is demonstrated using the composite of anomalous heat  
2 budget for five weak-to-moderate El Niño events (Figs. 9-10). The results, therefore,  
3 suggest that GODAS provides a reasonable estimate of both the seasonal cycle and  
4 interannual variability in the mixed layer heat budget. We conclude therefore that it is a  
5 useful tool for real-time monitoring of mixed layer variability and for further  
6 understanding of coupled ocean-atmospheric interactions.

7         The mixed layer heat budget analysis tool derived from GODAS can also be  
8 derived from other operational ocean reanalyses (ORA, hereafter) routinely produced by  
9 operational centers (Balmaseda et al. 20008; Oke et al. 2005; Alves and Robert 2005).  
10 The effort of deriving multi-model heat budget analyses would likely enhance our  
11 confidence in the feasibility of ORAs for monitoring and understanding tropical Pacific  
12 SST variability. Monitoring the differences among multi-model analyses will also help us  
13 identify common biases and deficiencies in ORAs and the requirements those ORAs  
14 impose on the ocean observing system for operational data streams (Xue et al. 2009). As  
15 the ORAs also provide initial conditions for seasonal climate predictions, the mixed layer  
16 budget analysis presented here can also be applied to understand the evolution of the SST  
17 anomalies in the forecast, as well as to understand the initial adjustments (sometimes  
18 referred to as initial shock) and development of coupled model biases.

19

## 20 **Acknowledgements**

21 We would like to thank Dr. Kelvin Richards, Dr. Shangping Xie, and an anonymous  
22 reviewer for their critical and constructive comments that helped us improve the  
23 manuscript significantly. We also want to thank Dr. David Behringer who provided us  
24 detailed information about the GODAS ocean analysis and for helpful discussions on our

1 results. This work was partially supported by the Climate Test Bed of NOAA and also by  
 2 NOAA's Climate Program Office.

3

#### 4 **Appendix A. Temperature equation**

5 The temperature equation for the mixed layer, described by Stevenson and Niiler,  
 6 (1983) is adopted here:

$$7 \quad h \frac{\partial T_a}{\partial t} = -h \bar{v}_a \cdot \nabla T_a - w_e \times (T_a - T_{-h}) - \nabla \cdot \left( \int_{-h}^0 \hat{v} \hat{T} dz \right) + (Q_O - Q_{pen} + Q_{corr} + Q_{diff}) / \rho c_p \quad (A1)$$

8 where  $h$  is MLD;  $T$  and  $\bar{v}$  are temperature and horizontal currents; the subscript  $a$   
 9 represents quantities that are vertically averaged quantities between the surface and  $h$ ;  $\hat{v}$   
 10 and  $\hat{T}$  in the third term on the right hand side are deviations from their vertically  
 11 averaged quantities, and their contribution to the heat budgets is generally very small in  
 12 the mixed layer (ZH08) and neglected in our discussions;  $w_e$  is the entrainment velocity  
 13 across the bottom of the mixed layer, which is calculated by

$$14 \quad w_e = \frac{\partial h}{\partial t} + \bar{v}_{-h} \cdot \nabla h + w_{-h} \quad (A2)$$

15 where  $w_{-h}$  is the vertical velocity at the bottom of the mixed layer. The last four terms in  
 16 Eq. (A1) are various heat flux terms.  $Q_O$  is the net downward surface heat fluxes that are  
 17 composed of shortwave ( $Q_{short}$ ) and longwave ( $Q_{long}$ ) radiation, latent ( $Q_{lh}$ ) and sensible  
 18 ( $Q_{sh}$ ) heat fluxes;  $Q_{pen}$  is the shortwave radiation flux that exits through the bottom of  
 19 MLD, and is parameterized (Pacanowski and Griffies 1999) as

$$20 \quad Q_{pen} = Q_{short} \left( 0.58e^{-\frac{h}{0.35}} + 0.42e^{-\frac{h}{23}} \right) \quad (A3)$$

1  $Q_{\text{corr}}$  represents a heat flux correction introduced by a relaxation of model SST to  
 2 observed SST in GODAS. Following Wang and McPhaden (1999), we define adjusted  
 3 net surface heat flux as

$$4 \quad Q_{\text{adj}} = Q_{\text{O}} - Q_{\text{pen}} + Q_{\text{corr}}. \quad (\text{A4})$$

5 The last term in the right hand of equation (A1),  $Q_{\text{diff}}$ , is the diffusive heat flux at the  
 6 bottom of the mixed layer, and is parameterized (Hayes et al. 1991) as:

$$7 \quad Q_{\text{diff}} = -\rho c_p K_z \frac{\partial T}{\partial z} \quad (\text{A5})$$

8 where  $\rho$  and  $c_p$  are density and heat capacity of sea water; and

$$9 \quad K_z = K_c + \frac{v}{1 + \beta \text{Ri}} \quad (\text{A6})$$

10 where  $K_c = 1 \times 10^{-5} \text{ m}^2 \text{ s}^{-1}$ ;  $\beta = 5$ ; Ri is the Richardson Number that is defined as

$$11 \quad \text{Ri} = \alpha g \frac{\partial T}{\partial z} \times \left[ \left( \frac{\partial u}{\partial z} \right)^2 + \left( \frac{\partial v}{\partial z} \right)^2 \right]^{-1} \quad (\text{A7})$$

12 where  $\alpha = 8.75 \times 10^{-6} (T + 9)$  in unit of  $(^\circ\text{C})^{-1}$  and  $g = 9.8 \text{ m s}^{-2}$ ; a minimum Ri is set to  
 13 -0.1 to ensure valid diagnosis; and  $v$  in equation (A6) is parameterized as

$$14 \quad v = v_c + v_0 \times (1 + \beta \text{Ri})^{-2} \quad (\text{A8})$$

15 where  $v_c = 1 \times 10^{-4} \text{ m}^2 \text{ s}^{-1}$  and  $v_0 = 3.5 \times 10^{-3} \text{ m}^2 \text{ s}^{-1}$ . We should point out that the  
 16 diffusion parameterization used in our analysis in (A5)-(A8) is much simpler than  
 17 originally implemented in GODAS (the K-profile parameterization (KPP) vertical mixing  
 18 scheme, Large et al. 1994), which may result in the imbalance of heat budgets.  
 19 Horizontal diffusion has been neglected due to its small magnitude.

1 We also note that vertical entrainment and diffusion are sometimes treated as a  
 2 residual to keep the closure of mixed layer heat budgets (WM99). They were often  
 3 combined and parameterized to be proportional to vertical differences between the  
 4 temperatures in and below the mixed layer. One common parameterization is to assume a  
 5 constant temperature difference of 1-4°C (see reference cited in WM99). An alternative  
 6 parameterization is to assume a depth from which colder water is entrained into the  
 7 mixed layer. The entrainment depth of 0-20 m below the mixed layer is used in many  
 8 studies (Stevenson and Niiler 1983; WM99; McPhaden et al 2008).

9 Following Zhang et al. (2007), the vertical entrainment is rewritten as

10  $w_e \frac{T_a - T_{-h}}{h} \equiv -w_e \frac{\partial T}{\partial z}$ . The Eq. (A1) then becomes

$$11 \quad \frac{\partial T_a}{\partial t} = -\bar{v}_a \cdot \nabla T_a - w_e \frac{\partial T}{\partial z} + \frac{Q_{adj}}{\rho c_p h} + \frac{Q_{diff}}{\rho c_p h} \quad (A9)$$

12 The equation (A9) can be rewritten as

$$13 \quad T_t = F \quad (A10)$$

$$14 \quad F = Q_u + Q_v + Q_w + Q_q + Q_{zz} \quad (A11)$$

15 where  $T_t = \frac{\partial T_a}{\partial t}$  is referred to as the temperature tendency, and F is referred to as the

16 forcing. The forcing F is the sum of zonal advection ( $Q_u = -u \frac{\partial T_a}{\partial x}$ ), meridional

17 advection ( $Q_v = -v \frac{\partial T_a}{\partial y}$ ), vertical entrainment ( $Q_w = -w_e \frac{\partial T}{\partial z}$ ), adjusted surface heat

18 flux ( $Q_q = \frac{Q_{adj}}{\rho c_p h}$ ), and vertical diffusion ( $Q_{zz} = \frac{Q_{diff}}{\rho c_p h}$ ). The consistency between  $T_t$  and

19 F can be used to check the closure of the temperature equation.

1

## 2 **Appendix B. Decomposition of temperature equation**

3 Following Kessler et al. (1998), each variable associated with forcing  $F$  is  
 4 decomposed into its low ( $\geq 75$  day) and high frequency components: for example,  
 5  $u = u_L + u_H$ . With this decomposition by omitting the subscript  $a$  in Eq. (A11), is written  
 6 as

$$7 \quad T_t = Q_u^L + Q_v^L + Q_w^L + Q_q^L + Q_{zz}^L + R_u + R_v + R_w + R_q + R_{zz} \quad (B1)$$

8 Where superscript L indicates the term calculated using low-pass filtered variables:

$$9 \quad Q_u^L = -u^L \frac{\partial T^L}{\partial x}, \quad Q_v^L = -v^L \frac{\partial T^L}{\partial y}, \quad Q_w^L = -w_e^L \frac{\partial T^L}{\partial z}, \quad Q_q^L = Q_q(Q_{adj}^L, h^L), \quad \text{and}$$

10  $Q_{zz}^L = Q_{zz}(Q_{diff}^L, h^L)$ .  $R$  in equation (B1) indicates the residue terms that involve high  
 11 frequency variations:

$$12 \quad R_u = -u^L \frac{\partial T^H}{\partial x} - u^H \frac{\partial T^L}{\partial x} - u^H \frac{\partial T^H}{\partial x}, \quad R_v = -v^L \frac{\partial T^H}{\partial y} - v^H \frac{\partial T^L}{\partial y} - v^H \frac{\partial T^H}{\partial y},$$

$$13 \quad R_w = -w^L \frac{\partial T^H}{\partial z} - w^H \frac{\partial T^L}{\partial z} - w^H \frac{\partial T^H}{\partial z}, \quad R_q = Q_q(Q_{adj}, h) - Q_q(Q_{adj}^L, h^L), \quad \text{and}$$

14  $R_{zz} = Q_{zz}(Q_{diff}, h) - Q_{zz}(Q_{diff}^L, h^L)$ . The residual terms are combined as an ‘‘eddy’’ term:

$$15 \quad E = R_u + R_v + R_w + R_q + R_{zz} \quad (B2)$$

16 Therefore, equation (B1) becomes

$$17 \quad T_t = Q_u^L + Q_v^L + Q_w^L + Q_q^L + Q_{zz}^L + E \quad (B3)$$

18 Eq. (B3) is further decomposed into climatology (bar) and its anomaly (prime).

19 The equation for anomalous temperature is, by omitting superscript L,

$$20 \quad T'_t = Q'_u + Q'_v + Q'_q + Q'_w + Q'_{zz} + E' \quad (B4)$$

1 Where

$$2 \quad Q'_u = -\bar{u} \frac{\partial \Gamma'}{\partial x} - u' \frac{\partial \bar{\Gamma}}{\partial x} - u' \frac{\partial \Gamma'}{\partial x} + \overline{u' \frac{\partial \Gamma'}{\partial x}} \quad (\text{B5})$$

$$3 \quad Q'_v = -\bar{v} \frac{\partial \Gamma'}{\partial y} - v' \frac{\partial \bar{\Gamma}}{\partial y} - v' \frac{\partial \Gamma'}{\partial y} + \overline{v' \frac{\partial \Gamma'}{\partial y}} \quad (\text{B6})$$

$$4 \quad Q'_q = Q_q - \bar{Q}_q \quad (\text{B7})$$

5 We combine vertical diffusion into the entrainment in equation (B4) because both  
6  $Q_w$  and  $Q_{zz}$  are parameterized to be proportional to the vertical gradient of temperature.

7 The vertical diffusion  $Q_{zz} = -\frac{K_z}{h} \frac{\partial T}{\partial z}$  is rewritten as  $Q_{zz} = -\omega \frac{\partial T}{\partial z}$ . Here,  $\omega = \frac{K_z}{h}$

8 represents an equivalent entrainment velocity and can be decomposed into its climatology

9 and anomaly:  $\omega = \bar{\omega} + \omega'$ . Therefore,  $Q'_{zz} = -\bar{\omega} \frac{\partial \Gamma'}{\partial z} - \omega' \frac{\partial \bar{\Gamma}}{\partial z} - \omega' \frac{\partial \Gamma'}{\partial z} + \overline{\omega' \frac{\partial \Gamma'}{\partial z}}$ .

10 The combination of anomalous vertical entrainment and vertical diffusive heat fluxes  
11 becomes,

$$12 \quad Q'_w + Q'_{zz} = -\bar{W} \frac{\partial \Gamma'}{\partial z} - W' \frac{\partial \bar{\Gamma}}{\partial z} - W' \frac{\partial \Gamma'}{\partial z} + \overline{W' \frac{\partial \Gamma'}{\partial z}} \quad (\text{B8})$$

13 where  $\bar{W} \frac{\partial \Gamma'}{\partial z} = \bar{w}'_e \frac{\partial \Gamma'}{\partial z} + \bar{\omega} \frac{\partial \Gamma'}{\partial z}$ ,  $W' \frac{\partial \bar{\Gamma}}{\partial z} = w'_e \frac{\partial \bar{\Gamma}}{\partial z} + \omega' \frac{\partial \bar{\Gamma}}{\partial z}$ ,  $W' \frac{\partial \Gamma'}{\partial z} = w'_e \frac{\partial \Gamma'}{\partial z} + \omega' \frac{\partial \Gamma'}{\partial z}$ , and

$$14 \quad \overline{W' \frac{\partial \Gamma'}{\partial z}} = \overline{w'_e \frac{\partial \Gamma'}{\partial z}} + \overline{\omega' \frac{\partial \Gamma'}{\partial z}}.$$

15 Finally, the anomalous heat by eddy is calculated as

$$16 \quad E' = E - \bar{E}. \quad (\text{B9})$$

1 **References**

- 2
- 3 An, S.-I., 2008: Interannual variations of the tropical ocean instability wave and ENSO.  
4 *J. Climate*, **21**, 3680-3686.
- 5 An, S.-I., and F.-F. Jin, 2001: Collective Role of Thermocline and Zonal Advective  
6 Feedbacks in the ENSO Mode. *J. Climate*, **14**, 3421-3432.
- 7 Alves, O., and C. Robert, 2005: Tropical Pacific ocean model error covariances from  
8 Monte Carlo simulations. *Q. J. R. Meteorol. Soc.*, **131**, 3643-3658.
- 9 Ando, K., and M. J. McPhaden, 1997: Variability of surface layer hydrography in the  
10 tropical Pacific Ocean. *J. Geophys. Res.*, **102**, 23 063–23 078.
- 11 Argo Science Team, 2001: *The global array of profiling floats, Observing the Ocean in*  
12 *the 21st Century*. C. J. Koblinsky and N.R. Smith, Eds., Australian Bureau of  
13 Meteorology, 248-258.
- 14 Balmaseda, M.A., A. Vidard, and D. Anderson, 2008: The ECMWF ORA-S3 ocean  
15 analysis system. *Mon. Wea. Rev.*, **136**, 3018-3034.
- 16 Behringer, D. W., Ji, M., and A. Leetmaa, 1998: An improved coupled model for ENSO  
17 prediction and implications for ocean initialization. Part I: The ocean data  
18 assimilation system. *Mon. Wea. Rev.*, **126**, 1013-1021.
- 19 Behringer, D. W., and Y. Xue, 2004: Evaluation of the global ocean data assimilation  
20 system at NCEP: The Pacific Ocean, Eighth Symposium on Integrated Observing  
21 and Assimilation System for Atmosphere, Ocean, and Land Surface, AMS 84<sup>th</sup>  
22 Annual Meeting, Washington State Convention and Trade Center, Seattle,  
23 Washington, 11-15.

- 1 Behringer, D. W., 2007: The Global Ocean Data Assimilation System at NCEP, *11th*  
2 *Symposium on Integrated Observing and Assimilation Systems for Atmosphere,*  
3 *Oceans, and Land Surface, AMS 87th Annual Meeting.* Henry B. Gonzales  
4 Convention Center, San Antonio, Texas, 12pp.
- 5 Bonjean, F. and G.S.E. Lagerloef, 2002: Diagnostic Model and Analysis of the Surface  
6 Currents in the Tropical Pacific Ocean. *J. Phys. Oceanogr.*, **32**, 2938-2954.
- 7 Chang, P., L. Ji, B. Wang, and T. Li, 1995: Interactions between the Seasonal Cycle and  
8 El Niño-Southern Oscillation in an Intermediate Coupled Ocean-Atmosphere  
9 Model. *J. Atmos. Sci.*, **52**, 353–2372.
- 10 Chen, D., A. J. Busalacchi, and L. M. Rothstein, 1994: The roles of vertical mixing,  
11 solar radiation, and wind stress in a model simulation of the sea surface  
12 temperature seasonal cycle in the tropical Pacific Ocean. *J. Geophys. Res.*, **98**  
13 20,345-20,359.
- 14 Conkright, M. E., S. Levitus, T. O'Brien, T. P. Boyer, C. Stephens, D. Johnson, O.  
15 Baranova, J. Antonov, R. Gelfeld, J. Rochester, C. Forgy, 1999: *World Ocean*  
16 *Database 1998, Documentation and Quality Control Version 2.0, National*  
17 *Oceanographic Data Center Internal Report 14*, National Oceanographic Data  
18 Center, Silver Spring, Maryland.
- 19 Contreras, R. F., 2002: Long-term observations of tropical instability waves. *J. Phys.*  
20 *Oceanogr.*, **32**, 2715-2722.
- 21 Derber, J., and A. Rosati, 1989: A global oceanic data assimilation system. *J. Phys.*  
22 *Oceanogr.* **19**, 1333-1347.

1 Frankignoul, C., F. Bonjean, and G. Reverdin, 1996): Interannual variability of surface  
2 currents in the tropical Pacific during 1987-1993. *J. Geophys. Res.*, **101**, 3629-  
3 3647.

4 Galanti E., and E. Tziperman, 2000: ENSO's Phase Locking to the Seasonal Cycle in the  
5 Fast-SST, Fast-Wave, and Mixed-Mode Regimes. *J. Atmos. Sci.*, **57**, 2936-2950.

6 Gent, P. R., and J. C. McWilliams, 1990: Isopycnal mixing in ocean circulation model, *J.*  
7 *Phys. Oceanogr.*, **20**, 150-155.

8 Hayes, S. P., P. Chang, and M. J. McPhaden, 1991: Variability of the sea surface  
9 temperature in the eastern equatorial Pacific during 1986-1988. *J. Geophys. Res.*  
10 **96**, 10,533-10,566.

11 Harrison, D. E., B. S. Giese, and E. S. Sarachik, 1990: Mechanisms of SST Change in  
12 the Equatorial Waveguide during the 1982–83 ENSO. *J. Climate*, **3**, 173–188.

13 Huang, B., Y. Xue, and D. W. Behringer, 2008: Impacts of Argo salinity in NCEP Global  
14 Ocean Data Assimilation System: The tropical Indian Ocean. *J. Geophys. Res.*,  
15 **113**, C08002, doi:10.1029/2007JC004388.

16 Ji, M., A. Leetmaa, and J. Derber, 1995: An ocean analysis system for seasonal to  
17 interannual climate studies. *Mon. Wea. Rev.*, **123**, 460-481.

18 Ji, M., R. W. Reynolds, and D. W. Behringer, 2000: Use of TOPEX/Poseidon sea level  
19 data for ocean analyses and ENSO prediction: Some early results. *J. Climate*, **13**,  
20 216-231.

21 Jin, F.-F., 1997: An equatorial ocean recharge paradigm for ENSO. Part I: Conceptual  
22 model. *J. Atmos. Sci.*, **54**, 811-829.

- 1 Jin, F.-F, S.-I. An, A. Timmermann, and J. Zhao, 2003: Strong El Niño events and  
2 nonlinear dynamical heating. *Geophys. Res. Lett.*, **30**, 1120, 18,  
3 doi:10.1029/2002GL016356.
- 4 Josey, S. A., E. C. Kent, and P. K. Taylor, 2002: Wind stress forcing of the ocean in the  
5 SOC climatology: Comparisons with the NCEP–NCAR, ECMWF,  
6 UWM/COADS, and Hellerman and Rosenstein Datasets. *J. Phys. Oceanogr.*, **32**,  
7 1993-2019
- 8 Jochum, M., and R. Murtugudde, 2006: Temperature advection by tropical instability  
9 waves. *J. Phys. Oceanogr.*, **36**, 592-605.
- 10 Kanamitsu, M., W. Ebisuzaki, J. Woolen, S.-K. Yang, J. J. Hnilo, M. Fiorino, and G. L.  
11 Potter, 2002: NCEP-DOE AMIP-II reanalysis (R-2). *Bull. Amer. Meteor. Soc.*, **83**,  
12 1631-1643.
- 13 Kessler, W. S., and M. J. McPhaden, 1995: The 1991-93 El Niño in the central Pacific.  
14 *Deep-Sea Research*, **42**, 295-333.
- 15 Kessler, W. S., L. M. Rothstein, and D. Chen, 1998: The annual cycle of SST in the  
16 eastern tropical Pacific, Diagnosed in an ocean GCM. *J. Climate*, **11**, 777-799.
- 17 Kim, S.-B., T. Lee, and I. Fukumori, 2007: Mechanisms controlling the interannual  
18 variation of mixed layer temperature averaged over the Niña-3 region. *J. Climate*  
19 **20**, 3822-3843.
- 20 Large, W. G., J. C. McWilliams, and S. C. Doney, 1994: Oceanic vertical mixing: A  
21 review and a model with nonlocal boundary layer parameterization. *Rev.*  
22 *Geophys.*, **32**, 363-403.
- 23 Lee, T. , I. Fukumori, and B. Tang, 2004: Temperature Advection: Internal versus  
24 External Processes. *J. Phys. Oceanogr.*, **34**, 1936-1944.

1 McPhaden, M.J., M.F. Cronin, and D.C. McClurg, 2008: Meridional structure of the  
2 surface mixed layer temperature balance on seasonal time scales in the eastern  
3 tropical Pacific. *J. Climate*, **21**, 3240-3260.

4 McPhaden, M. J., and X. Zhang, 2009: Asymmetry in zonal phase propagation of ENSO  
5 sea surface temperature anomalies. *Geophys. Res. Lett.*, **36**, L13703,  
6 doi:10.1029/2009GL038774.

7 Menkes, C.E., J.G. Vialard, and S.C. Kennan, J.P. Boulanger, and G. V. Madec, 2006: A  
8 modeling study of the impact of tropical instability waves on the heat budget of  
9 the eastern equatorial Pacific. *J. Phys. Oceanogr.*, **36**, 847-865.

10 Mitchell, T.P, and J.M. Wallace, 1992: The annual cycle in equatorial convection and sea  
11 surface temperature, *J. Climate*, **5**, 1140-1156.

12 Oke, P. R., A. Schiller, D. A. Griffin, and G. B. Brassington, 2005: Ensemble data  
13 assimilation for an eddy-resolving ocean model of the Australian region. *Q. J.*  
14 *Roy. Met. Soc.*, **131**, 3301-3311.

15 Pacanowski, R. C., and S. M. Griffies, 1999: *MOM 3.0 Manual*. NOAA/Geophysical  
16 Fluid Dynamics Laboratory, Princeton, New Jersey, 668 pp.

17 Picaut, J, M. Ioualalen, C. Menkes, T. Delcroix, and M. J. McPhaden, 1996: Mechanism  
18 of the zonal displacements of the Pacific Warm Pool: Implications for ENSO.  
19 *Science*, **29**, DOI: 10.1126/science.274.5292.1486.

20 Philander, S. G. H., W. J. Hurlin, and R.C. Pacanowski, 1986: Properties of long  
21 equatorial waves in the models of seasonal cycle in the tropical Atlantic and  
22 Pacific Oceans. *J. Geophys. Res.*, **91**, 14,207-14,211.

23 Philander, S. G., 1990: El Nino, La Nina, and the Southern Oscillation. *Academic Press*.  
24 pp 293.

1 Rasmusson, E. M., and T. H. Carpenter, 1982: Variations in tropical sea surface  
2 temperature and surface wind fields associated with the Southern Oscillation/El  
3 Niño. *Mon. Wea. Rev.*, **110**, 354–384.

4 Reynolds, R. W., N. A. Rayner, T. M. Smith, D. C. Stokes and W. Wang, 2002: An  
5 improved in situ and satellite SST analysis for climate. *J. Climate*, **15**, 1609-1625.

6 Richards, K.J., S.-P. Xie, and T. Miyama, 2009: Vertical mixing in the ocean and its impact on the  
7 coupled ocean-atmosphere system in the Eastern Tropical Pacific. *J. Climate*, **22**, 3703–3719.

8 Saha, S., S. Nadiga, C. Thiaw, J. Wang, W. Wang, Q. Zhang, H. M. van den Dool, H.-L.  
9 Pan, S. Moorthi, D. Behringer, D. Stokes, G. White, S. Lord, W. Ebisuzaki, P.  
10 Peng, and P. Xie, 2006: The NCEP climate forecast system. *J. Climate*, **19**, 3483-  
11 3517.

12 Seo K.-H. , and Y. Xue, 2005: MJO-related oceanic Kelvin waves and the ENSO cycle:  
13 A study with the NCEP Global Ocean Data Assimilation System. *Geophys. Res.*  
14 *Let.* **32**, L07712, doi:10.1029/2005GL022511.

15 Seager, R., 1989: Modeling tropical Pacific sea surface temperature: 1970-87. *J. Phys.*  
16 *Oceanogr.*, **19**, 419-434.

17 Shaji, c., C. Wang, G.R. Halliwell, and A. Wallcraft, 2005: Simulation of tropical Pacific  
18 and Atlantic Oceans using a HYbrid Coordinate Ocean Model. *Ocean Modelling*,  
19 **9**, 253–282.

20 Smith, T. M., R. W. Reynolds, T. C. Peterson, and J. Lawrimore, 2008: Improvements  
21 to NOAA’s Historical Merged Land–Ocean Surface Temperature Analysis  
22 (1880–2006). *J. Climate*, **21**, 2283-2296.

23 Sprintall, J., and M. Tomczak, 1992: Evidence of the barrier layer in the surface layer of  
24 the tropics. *J. Geophys. Res.*, **97**, 7305-7316.

- 1 Stevenson, J. W., and Pearn P. Niiler, 1983: Upper ocean heat budget during the Hawaii-  
2 Tahiti Shuttle Experiment. *J. Phys. Oceanogr.*, **13**, 1894-1907.
- 3 Swenson, M. S., and D.V. Hansen, 1999: Tropical Pacific Ocean mixed layer heat  
4 budget: The Pacific cold tongue. *J. Phys. Oceanogr.*, **29**, 69-81.
- 5 Tziperman, E., M. A. Cane, S. E. Zebiak, Y. Xue and B. Blumenthal, 1998: Locking of  
6 El Nino's peak time to the end of the calendar year in the delayed oscillator  
7 picture of ENSO. *J. Climate*, **11**, 2191-2199.
- 8 Vialard, J., C. Menkes, J.-P. Boulanger, P. Delecluse, E. Guilyardi, M.J. McPhaden, G.  
9 Madec, 2001: A model study of oceanic mechanisms affecting equatorial Pacific  
10 sea surface temperature during 1997-1998 El Nino. *J. Phys. Oceanogr.*, **31**, 1649-  
11 1675.
- 12 Wang, W., M. J. McPhaden, 1999: The surface-layer heat balance in the equatorial  
13 Pacific Ocean. Part I: Mean seasonal cycle. *J. Phys. Oceanogr.*, **29**, 1812-1831.
- 14 Wang, W. and M. J. McPhaden, 2000: The Surface-Layer Heat Balance in the Equatorial  
15 Pacific Ocean. Part II: Interannual Variability. *J. Phys. Oceanogr.*, **30**, 2989-3008.
- 16 Wang, W., and M. J. McPhaden, 2001a: Surface layer temperature balance in the  
17 equatorial Pacific during the 1997-1998 El Nino and 1998-1999 La Nina. *J.*  
18 *Climate*, **14**, 3393-3407.
- 19 Wang, W. and M.J. McPhaden 2001b: What is the mean seasonal cycle of surface heat flux  
20 in the equatorial Pacific? *J. Geophys. Res.*, **106**, 837-857.
- 21 Xie, S.-P., 1994: On the genesis of the equatorial annual cycle. *J. Climate*, **7**, 2008-2013.  
22

- 1 Xue, Y., Alves, O., Balmaseda, M., Ferry, N., Good, S., Ishikawa, I., Lee, T., McPhaden,  
2 M., Peterson, D., & Rienecker, M., 2010: Ocean state estimation for global ocean  
3 monitoring: ENSO and beyond ENSO. In Proc. "OceanObs'09: Sustained Ocean  
4 Observations and Information for Society" Conference (Vol. 2), Venice, Italy, 21-  
5 25 September 2009, Hall, J., Harrison D.E. and Stammer, D., Eds., ESA  
6 Publication WPP-306.
- 7 You Y., 1995: Salinity variability and its role in the barrier-layer formation during  
8 TOGA-COARE. *J. Phys. Oceanogr.*, **25**, 2778-2807.
- 9 Yu, J. Y., W. T. Liu, 2003: A linear relationship between ENSO intensity and tropical  
10 instability wave activity in the eastern Pacific Ocean. *Geophys. Res. Lett.*, **30**,  
11 doi:10.1029/2003GL017176.
- 12 Yu, L., X. Jin, and R. A. Weller, 2008: Multidecade Global Flux Datasets from the  
13 Objectively Analyzed Air-sea Fluxes (OAFlux) Project: Latent and sensible heat  
14 fluxes, ocean evaporation, and related surface meteorological variables. *Woods  
15 Hole Oceanographic Institution, OAFlux Project Technical Report. OA-2008-01*,  
16 64pp. Woods Hole. Massachusetts.
- 17 Yuan, D., 2005: Role of the Kelvin and Rossby waves in the seasonal cycle of the  
18 equatorial Pacific Ocean circulation. *J. Geophys. Res.*, **110**, C04004,  
19 doi:10.1029/2004JC002344.
- 20 Zhang, Q., A. Kumar, Y. Xue, W. Wang, F.-F. Jin, 2007: Analysis of the ENSO cycle in  
21 the NCEP coupled forecast model. *J. Climate*, **20**, 1265-1284.
- 22 Zhang, X., 2008: Local forcing of sea surface temperature in the eastern equatorial  
23 Pacific on ENSO time scales. *Ph.D. Dissertation*. University of Washington.  
24 Seattle, Washington. 159pp.

- 1 Zhang, X. and M.J. McPhaden, 2006: Wind stress variations and interannual sea surface  
2 temperature anomalies in the eastern equatorial Pacific. *J. Climate*, **19**, 226-241.
- 3 Zhang, X. and M.J. McPhaden, 2008: Eastern equatorial Pacific forcing of ENSO sea surface  
4 temperature anomalies. *J. Climate*, **21**, 6070-6079.

1 **Table captions**

2

3 Table 1. Mean bias (MBIAS, positive towards east) ( $\text{cm s}^{-1}$ ), root mean square error  
4 (RMSE) ( $\text{cm s}^{-1}$ ), anomaly correlation coefficient (ACC), and anomaly RMSE  
5 (ARMSE), in which the mean biases were removed, of zonal currents between  
6 OSCAR and TAO, and between GODAS and TAO.

7 Table 2. Same as Table 1 except for meridional currents. Positive towards north for  
8 MBIAS.

1 **Figure captions**

2 Figure 1. Zonal current (93-07) at 15 m depth along the Equator (1°S-1°N) in (a) OSCAR,  
3 (b) GODAS, and (c) GODAS-OSCAR. CIs are  $10 \text{ cm s}^{-1}$

4 Figure 2. Zonal current ( $\text{cm s}^{-1}$ ) at (a) 165°E, (b) 170°W, (c) 140°W, and (d) 110°W;  
5 and meridional current ( $\text{cm s}^{-1}$ ) at (e) 165°E, (f) 170°W, (g) 140°W, and (h)  
6 110°W. Currents are at 10 m depth for GODAS and TAO from current meters,  
7 and at 15 m for OSCAR. Averaging periods for GODAS and TAO are 1986-  
8 2008, 2002-2008 1983-2008, and 1982-2004, respectively, at 165°E, 170°W,  
9 140°W, and 110°W. The averaging period for OSCAR is 1993-2007. A 6-pentad  
10 running mean has been applied in the plots.

11 Figure 3. Mixed layer depth (82-04) along the Equator (1°S-1°N) in (a) WOD01, (b)  
12 GODAS, and (c) GODAS-WOD01. The CIs are 10 m.

13 Figure 4. Heat budget closure of the mixed layer between  $T_i$  and F in NINO3.4 region  
14 (120°W-170°W, 5°S-5°N): Climatological temperature budget in CNTRL (a) and  
15 GODAS (c), and anomalous temperature budget in CNTRL (b) and GODAS (d).  
16 Units:  $^{\circ}\text{C mon}^{-1}$ . The temporal correlation coefficient and RMSE are 0.99 and  
17  $0.09^{\circ}\text{C mon}^{-1}$  in (a), 0.95 and  $0.10^{\circ}\text{C mon}^{-1}$  in (b), 0.97 and  $0.06^{\circ}\text{C mon}^{-1}$  in  
18 (c), and 0.70 and  $0.23^{\circ}\text{C mon}^{-1}$  in (d).

19 Figure 5. Heat fluxes of the equatorial (1°S-1°N) Pacific Ocean. (a) Downward solar  
20 radiation, (b) Downward longwave radiation, (c) Sensible heat, (d) Latent heat,  
21 (e) Penetrative solar radiation, (f) Corrected heat flux in GODAS, (g) Adjusted  
22 net heat flux, and (h) Difference of net surface heat flux between GODAS and  
23 OAFflux. CIs are 20, 5, 5 20, 10 20, and  $20 \text{ W m}^{-2}$ , respectively in (a), (b),  
24 (c), (d), (e), (f), (g), and (h). Contours are shaded above 220, 120, 30 20, and 60

1             $W m^{-2}$ , respective, in (a), (d), (e), (f) and (g); and shaded below -50 and -60  $W$   
2             $m^{-2}$  in (b) and (h).

3    Figure 6. Averaged (1982-2004) and low-pass filtered temperature budgets by (a) Zonal  
4            advection, (b) Meridional advection, (c) Entrainment, (d) Adjusted surface  
5            heating, and (e) Vertical diffusion. (f) Eddy. Contours are 0,  $\pm 0.2$ ,  $\pm 0.5$ ,  $\pm 1$ ,  
6             $\pm 1.5$ ,  $\pm 2$ , and  $\pm 3^{\circ}C mon^{-1}$ .

7    Figure 7. Low-pass filtered temperature budgets at  $0.5^{\circ}N$  by (a) Zonal advection, (b)  
8            Meridional advection, (c) Entrainment and vertical diffusion, and (d) Adjusted  
9            surface heating. (e) Unfiltered temperature tendency. (f) Eddy. Contours are 0,  
10            $\pm 0.5$ ,  $\pm 1$ ,  $\pm 1.5$ ,  $\pm 2$ ,  $\pm 3$ ,  $\pm 4$ , and  $\pm 5^{\circ}C mon^{-1}$ .

11   Figure 8. Unfiltered temperature budgets of the equatorial Pacific Ocean at  $110^{\circ}W$ ,  
12            $140^{\circ}W$ ,  $170^{\circ}W$ , and  $165^{\circ}E$ . (a) Temperature tendency, (b) Zonal advection, (c)  
13           Meridional advection, (d) Adjusted heat flux, and (e) Entrainment and vertical  
14           diffusion. Units:  $^{\circ}C mon^{-1}$ . A 6-pentad running mean has been applied in the  
15           plots.

16   Figure 9. Low-pass filtered temperature budgets of the El Niño composite between  $1^{\circ}S$   
17           and  $1^{\circ}N$  by (a) Zonal advection, (b) Meridional advection, (c) Entrainment and  
18           vertical diffusion, and (d) Adjusted surface heat. (e) Eddy between unfiltered and  
19           low-pass filtered budgets. (f) Unfiltered temperature tendency, (g) Unfiltered  
20           forcing in Eq (2), and (h) Unfiltered temperature. Contours are 0,  $\pm 0.2$ ,  $\pm 0.5$ ,  
21            $\pm 1$ ,  $\pm 1.5$  and  $\pm 2$ . Units are  $^{\circ}C mon^{-1}$  in (a)-(g) and  $^{\circ}C$  in (h). A 6-pentad  
22           running mean has been applied in the plots.

23   Figure 10. Temperature budget anomalies of the El Niño composite in NINO3.4 region  
24           ( $5^{\circ}S -5^{\circ}N$ ,  $120^{\circ}W-170^{\circ}W$ ). (a) Unfiltered temperature budgets ( $^{\circ}C mon^{-1}$ ).

1        Decomposition of low-pass filtered (b) Zonal advection, (c) Meridional advection,  
2        and (d) Entrainment and vertical diffusion. The unfiltered budgets in (a) are  
3        replotted in (b)-(d). Temperature anomalies are plotted in the scale of the right  
4        axis. Decomposed of climatology and associated anomaly are noted as bar and  
5        prime, for example,  $\overline{U} \bar{T}' = \bar{u} \cdot T'_x$  . The “Eddy” in (b)-(d) represents the  
6        difference between unfiltered budget anomaly in (a) and low-pass filtered budget  
7        anomaly.

8        Figure 11. (a) Components of surface heat flux anomalies (left axis) and MLD anomaly  
9        (right axis) of the El Niño composite in NINO3.4 region (5°S -5°N, 120°W-  
10        170°W). The fluxes are positive downward except for  $Q_{pen}$  that is positive  
11        upward. (b) Mixed layer heat budget closure (left axis) and mixed layer  
12        temperature anomaly (right axis) in NINO3.4 region.

13        Figure 12. Temperature budget anomalies at 110°W and 0°N from 1997 to 1998. (a)  
14        Unfiltered temperature budget (°C ) at 110°W and 0°N. Decomposition of low-  
15        pass filtered (b) Zonal advection, and (c) Meridional advection. (d) Zonal current  
16        of TAO and GODAS for 1997-98 El Niño event at 110°W, 0°N, and 35 m depth.  
17        A 5-month running mean and a 3-month running mean has been applied in (a)-(c),  
18        and a 3-month running mean has been applied in (d).

19        Figure 13. Same as Figure 12 except for the 1982-83 El Niño event.

1 Table 1. Mean biases (MBIAS, positive towards east) ( $\text{cm s}^{-1}$ ), root-mean-square-error  
 2 (RMSE) ( $\text{cm s}^{-1}$ ), anomalous correlation coefficients (ACC), and anomalous  
 3 RMSE (ARMSE), in which the means in each data sets were removed, of zonal  
 4 currents between OSCAR and TAO, and between GODAS and TAO.

	165°E		170°W		140°W		110°W	
	OSCAR	GODAS	OSCAR	GODAS	OSCAR	GODAS	OSCAR	GODAS
MBIAS	-18	-24	13	23	-4	13	-2	-18
RMSE	19	26	14	26	8	15	5	18
ACC	0.93	0.76	0.94	0.80	0.95	0.96	0.98	0.98
ARMSE	5	10	6	11	7	7	5	5

6  
7  
8  
9

10 Table 2. Same as Table 1 except for meridional currents. Positive towards north for  
 11 MBIAS.

	165°E		170°W		140°W		110°W	
	OSCAR	GODAS	OSCAR	GODAS	OSCAR	GODAS	OSCAR	GODAS
MBIAS	4	1	7	4	3	4	-2	-2
RMSE	4	2	8	4	4	4	2	3
ACC	0.07	0.59	0.05	0.90	-0.07	0.56	0.81	0.44
ARMSE	2	1	3	1	2	2	1	2

13  
14  
15

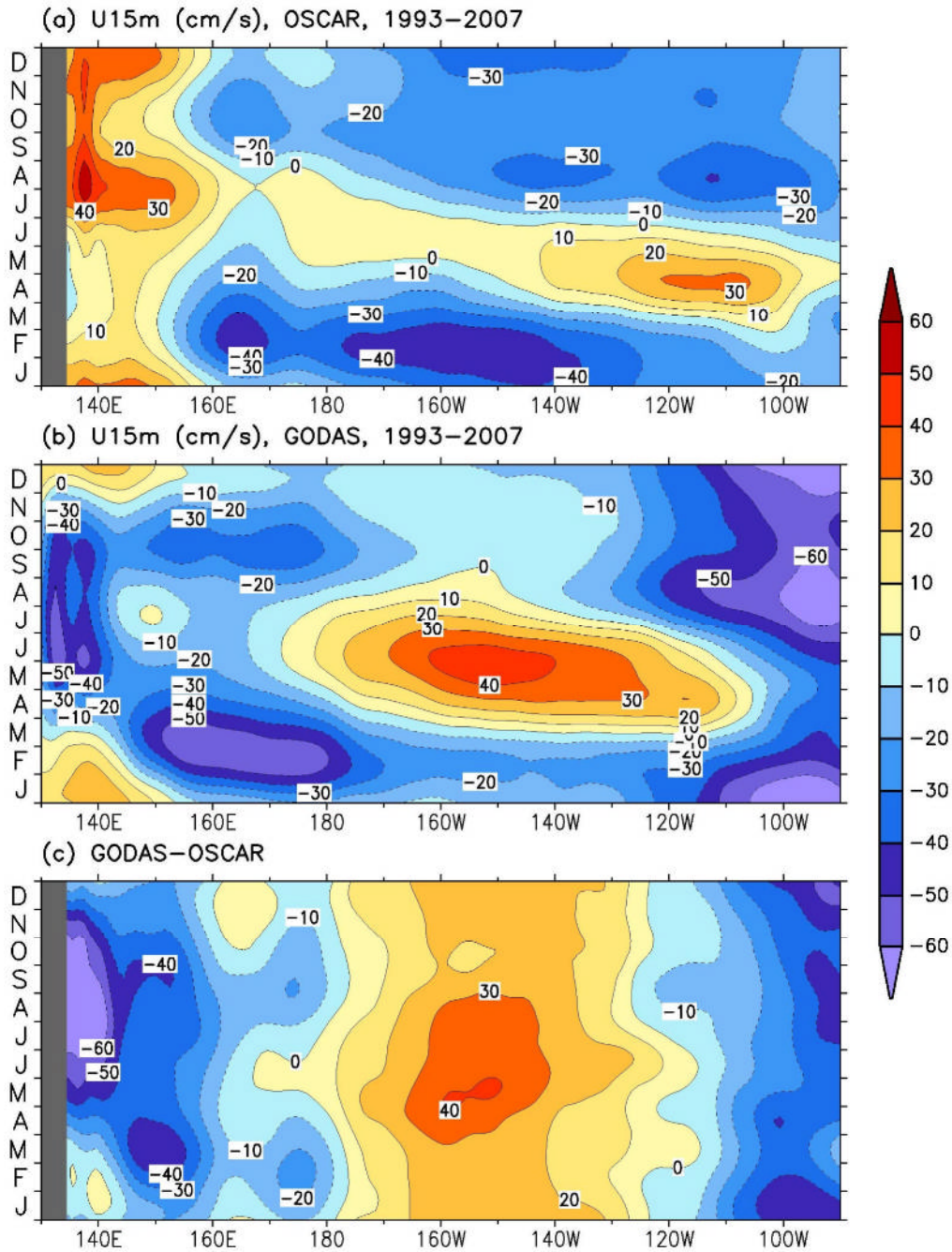


Figure 1. Zonal current (93-07) at 15 m depth along the Equator (1°S-1°N) in (a) OSCAR, (b) GODAS, and (c) GODAS-OSCAR. CIs are 10 cm s<sup>-1</sup>.

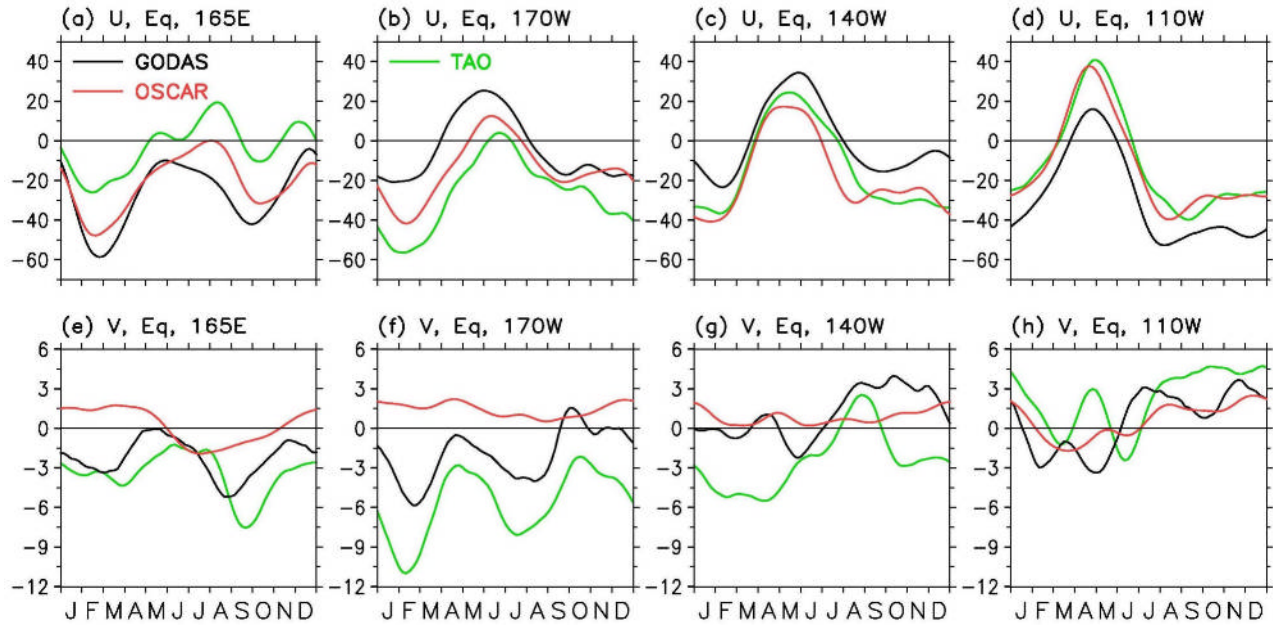


Figure 2. Zonal current ( $\text{cm s}^{-1}$ ) at (a)  $165^{\circ}\text{E}$ , (b)  $170^{\circ}\text{W}$ , (c)  $140^{\circ}\text{W}$ , and (d)  $110^{\circ}\text{W}$ ; and meridional current ( $\text{cm s}^{-1}$ ) at (e)  $165^{\circ}\text{E}$ , (f)  $170^{\circ}\text{W}$ , (g)  $140^{\circ}\text{W}$ , and (h)  $110^{\circ}\text{W}$ . Currents are at 10 m depth for GODAS and TAO from current meters, and at 15 m for OSCAR. Averaging periods for GODAS and TAO are 1986-2008, 2002-2008, 1983-2008, and 1982-2004, respectively, at  $165^{\circ}\text{E}$ ,  $170^{\circ}\text{W}$ ,  $140^{\circ}\text{W}$ , and  $110^{\circ}\text{W}$ . The averaging period for OSCAR is 1993-2007. A 6-pentad running mean has been applied in the plots.

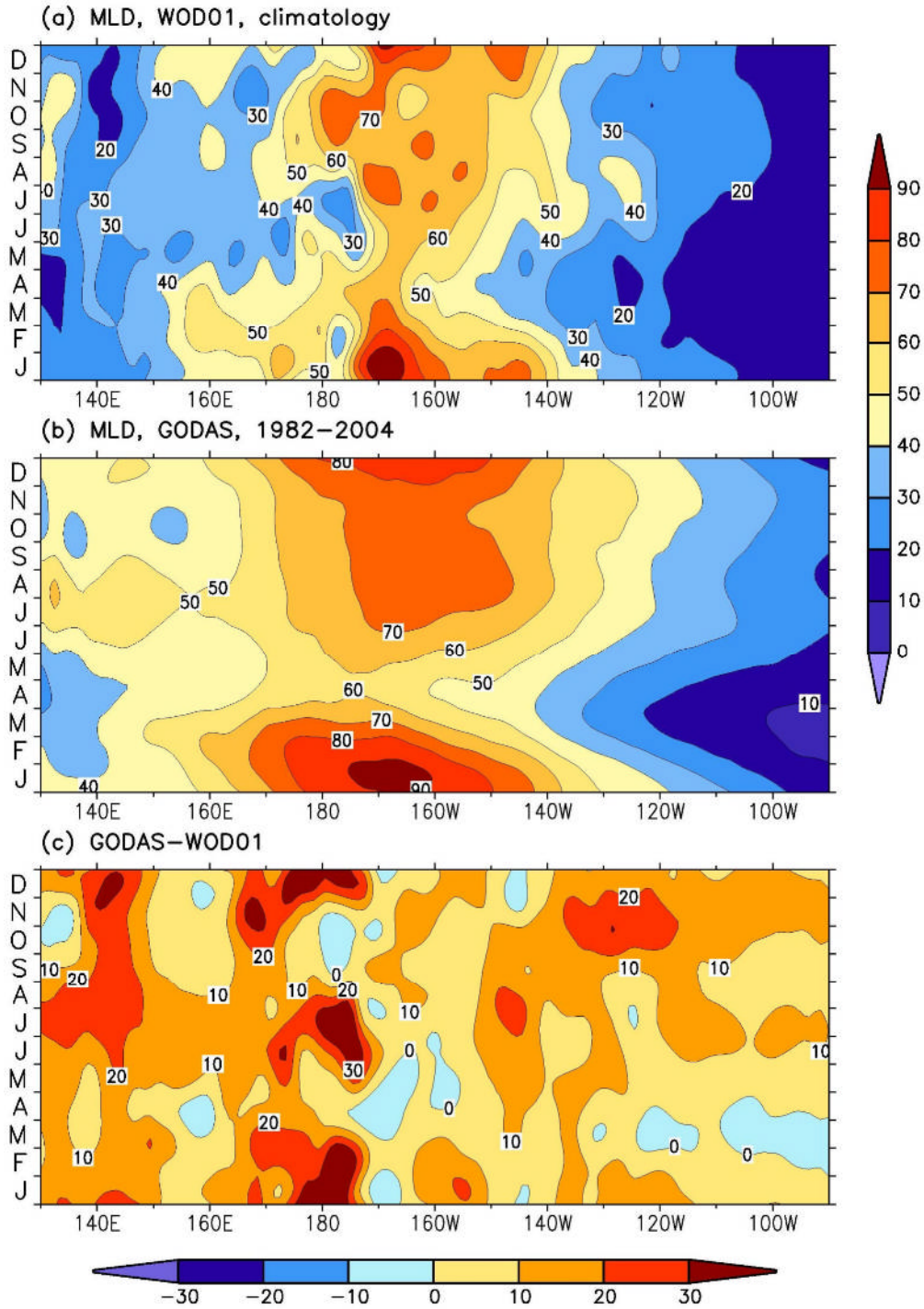


Figure 3. Mixed layer depth (82-04) along the Equator (1°S-1°N) in (a) WOD01, (b) GODAS, and (c) GODAS-WOD01. The CIs are 10 m.

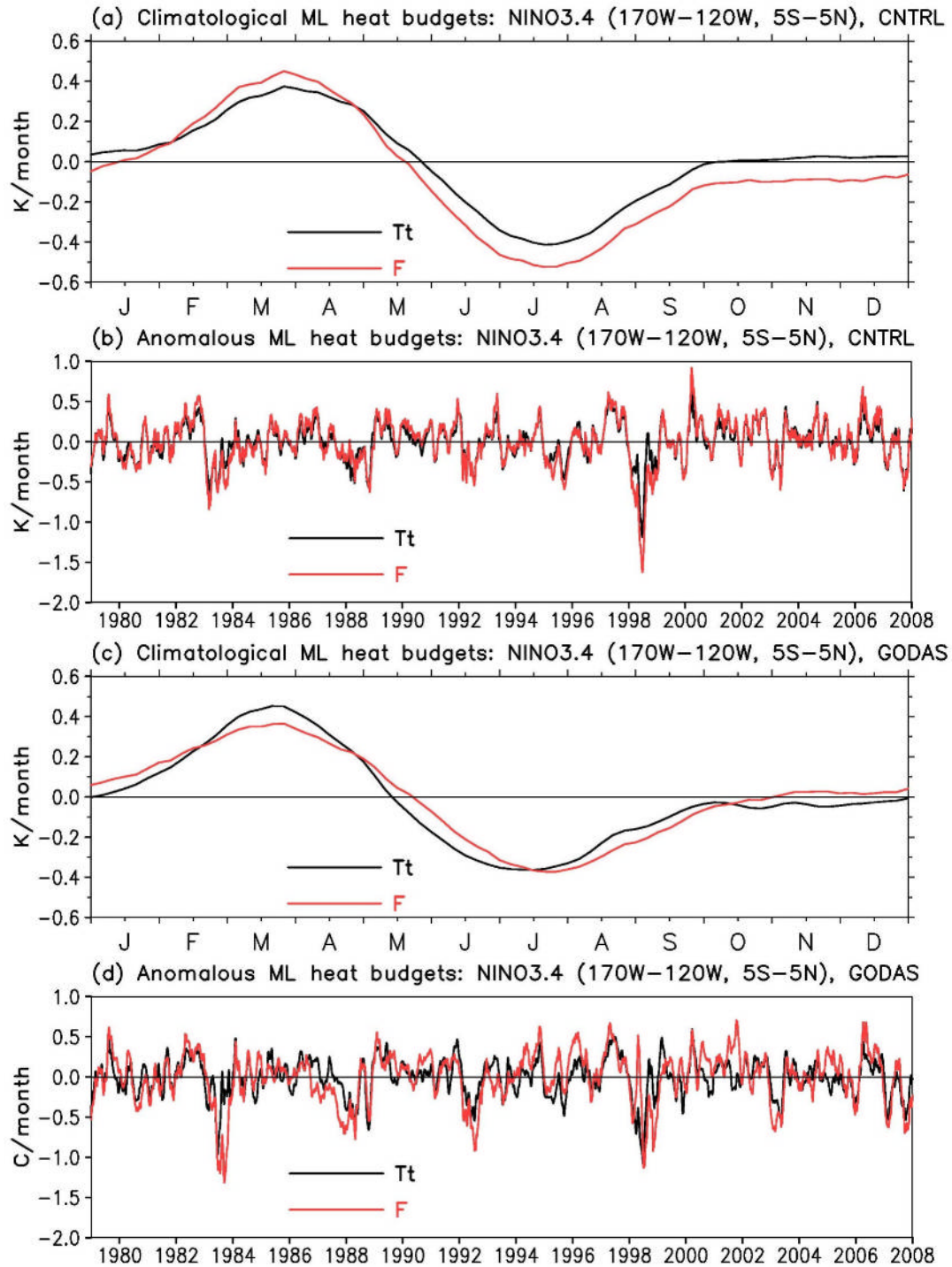


Figure 4. Heat budget closure of the mixed layer between  $T_t$  and  $F$  in NINO3.4 region (120°W-170°W, 5°S-5°N): Climatological temperature budget in CNTRL (a) and GODAS (c), and anomalous temperature budget in CNTRL (b) and GODAS (d). Units:  $^{\circ}\text{C mon}^{-1}$ . The temporal correlation coefficient and RMSE are 0.99 and  $0.09^{\circ}\text{C mon}^{-1}$  in (a), 0.95 and  $0.10^{\circ}\text{C mon}^{-1}$  in (b), 0.97 and  $0.06^{\circ}\text{C mon}^{-1}$  in (c), and 0.70 and  $0.23^{\circ}\text{C mon}^{-1}$  in (d).

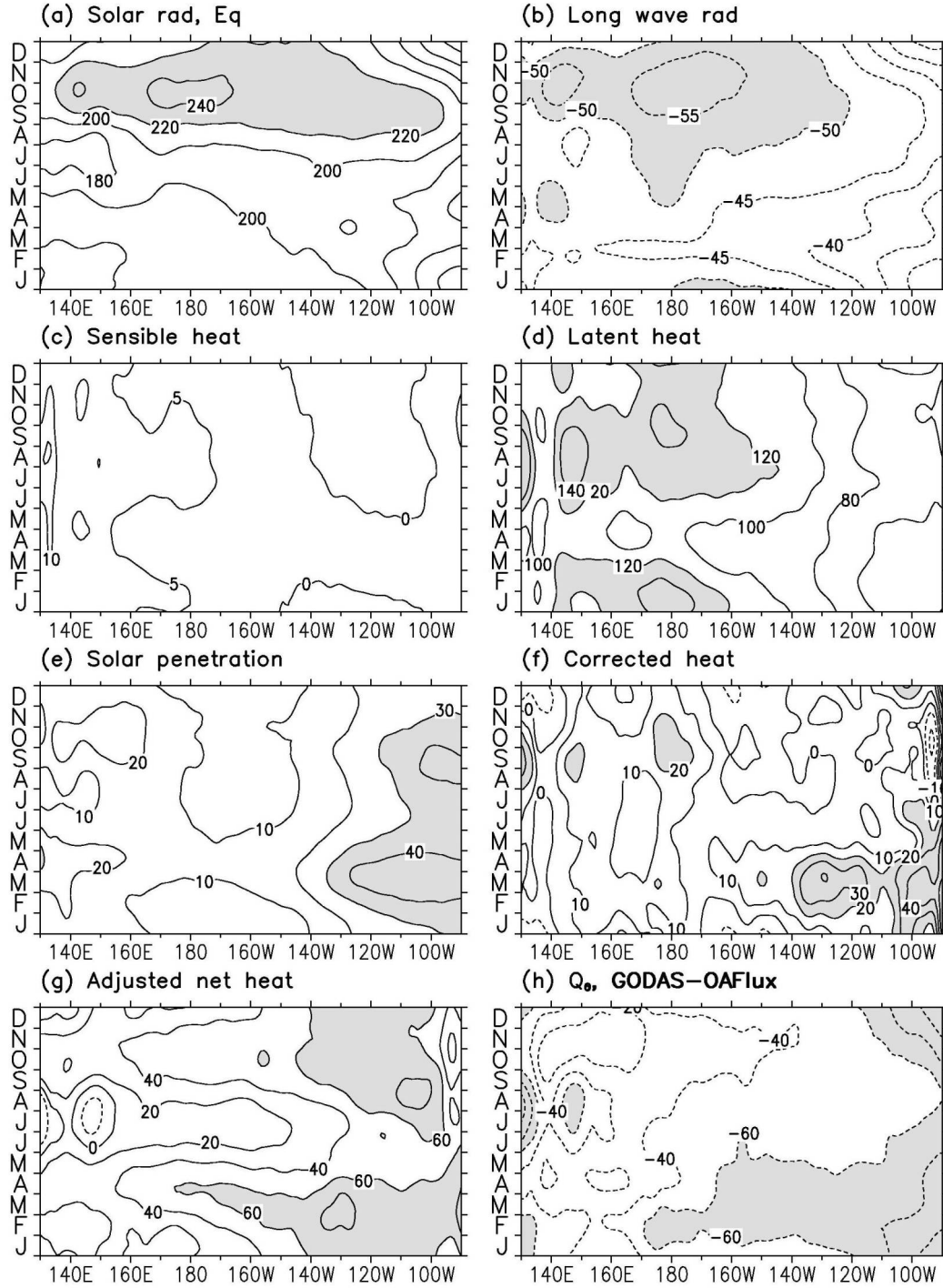


Figure 5. Heat fluxes of the equatorial ( $1^{\circ}\text{S}$ - $1^{\circ}\text{N}$ ) Pacific Ocean. (a) Downward solar radiation, (b) Downward longwave radiation, (c) Sensible heat, (d) Latent heat, (e) Penetrative solar radiation, (f) Corrected heat flux in GODAS, (g) Adjusted net heat flux, and (h) Difference of net surface heat flux between GODAS and OAFlux. CIs are 20, 5, 5, 20, 10, 10, 20, and 20  $\text{W m}^{-2}$ , respectively in (a), (b), (c), (d), (e), (f), (g), and (h). Contours are shaded above 220, 120, 30, 20, and 60  $\text{W m}^{-2}$ , respective, in (a), (d), (e), (f) and (g); and shaded below  $-50$  and  $-60$   $\text{W m}^{-2}$  in (b) and (h).

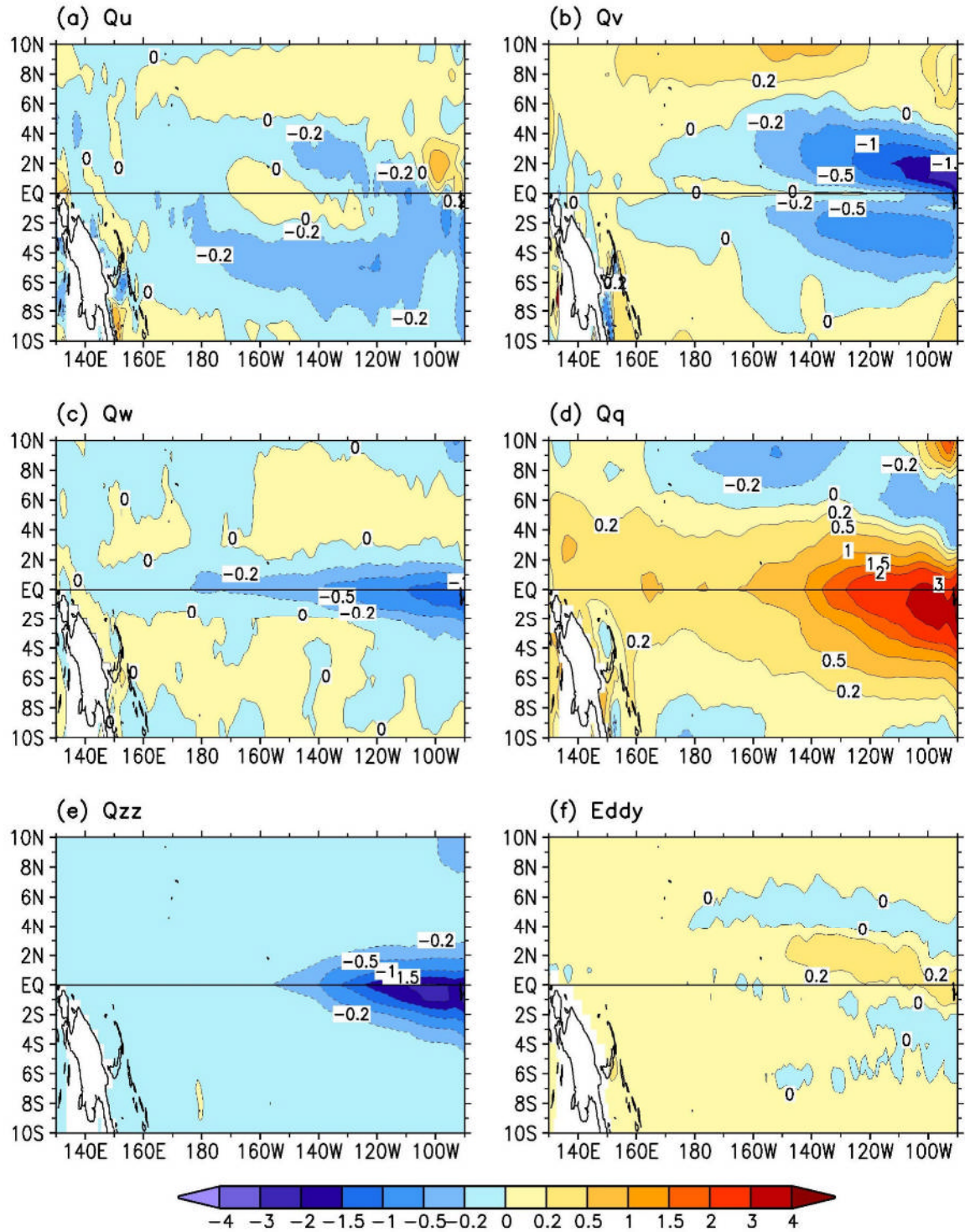


Figure 6. Averaged (1982-2004) and low-pass filtered temperature budgets by (a) Zonal advection, (b) Meridional advection, (c) Entrainment, (d) Adjusted surface heating, and (e) Vertical diffusion. (f) Eddy. Contours are 0,  $\pm 0.2$ ,  $\pm 0.5$ ,  $\pm 1$ ,  $\pm 1.5$ ,  $\pm 2$ , and  $\pm 3^{\circ}\text{C mon}^{-1}$ .

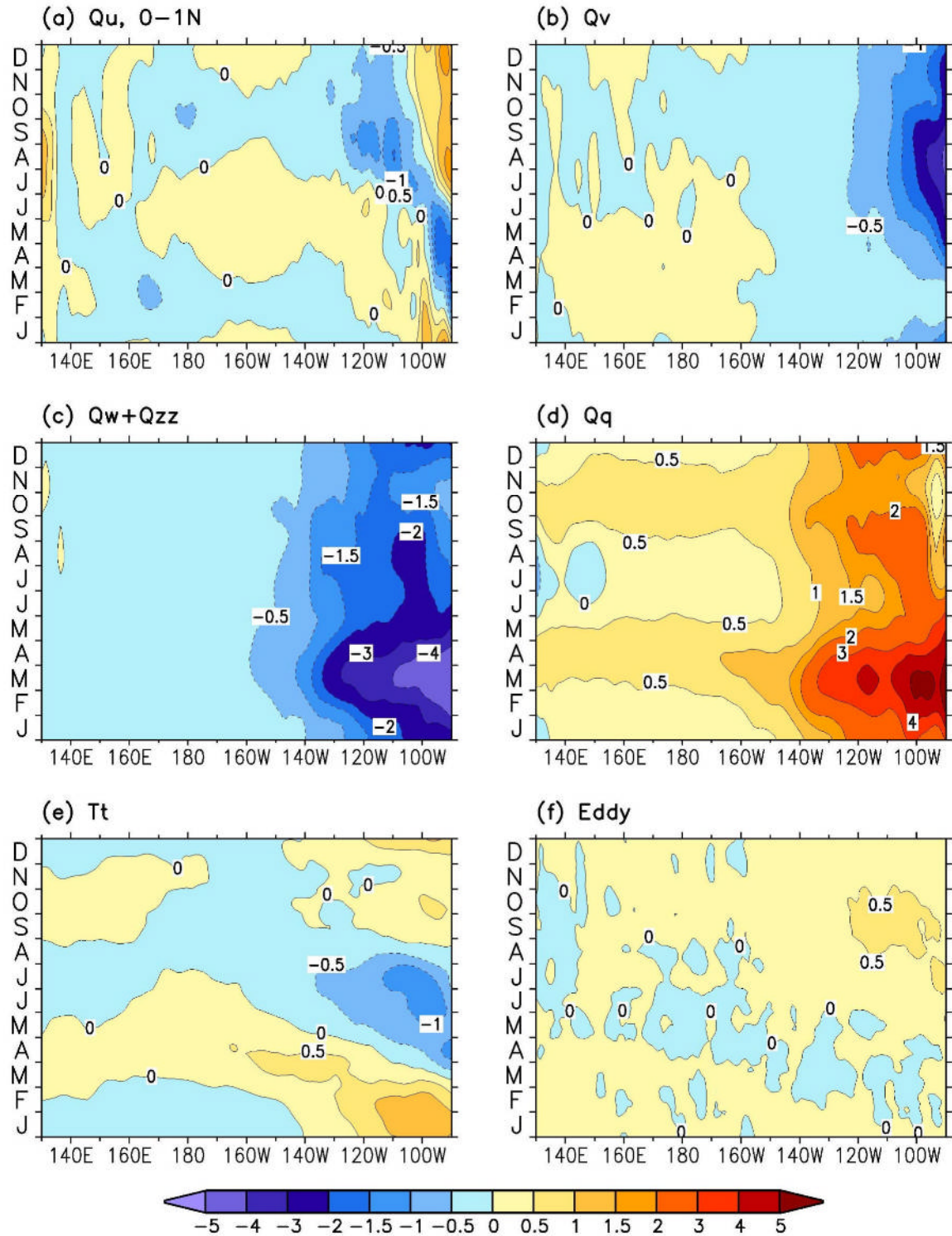


Figure 7. Low-pass filtered temperature budgets at 0.5°N by (a) Zonal advection, (b) Meridional advection, (c) Entrainment and vertical diffusion, and (d) Adjusted surface heating. (e) Unfiltered temperature tendency. (f) Eddy. Contours are 0,  $\pm 0.5$ ,  $\pm 1$ ,  $\pm 1.5$ ,  $\pm 2$ ,  $\pm 3$ ,  $\pm 4$ , and  $\pm 5^\circ\text{C mon}^{-1}$ .

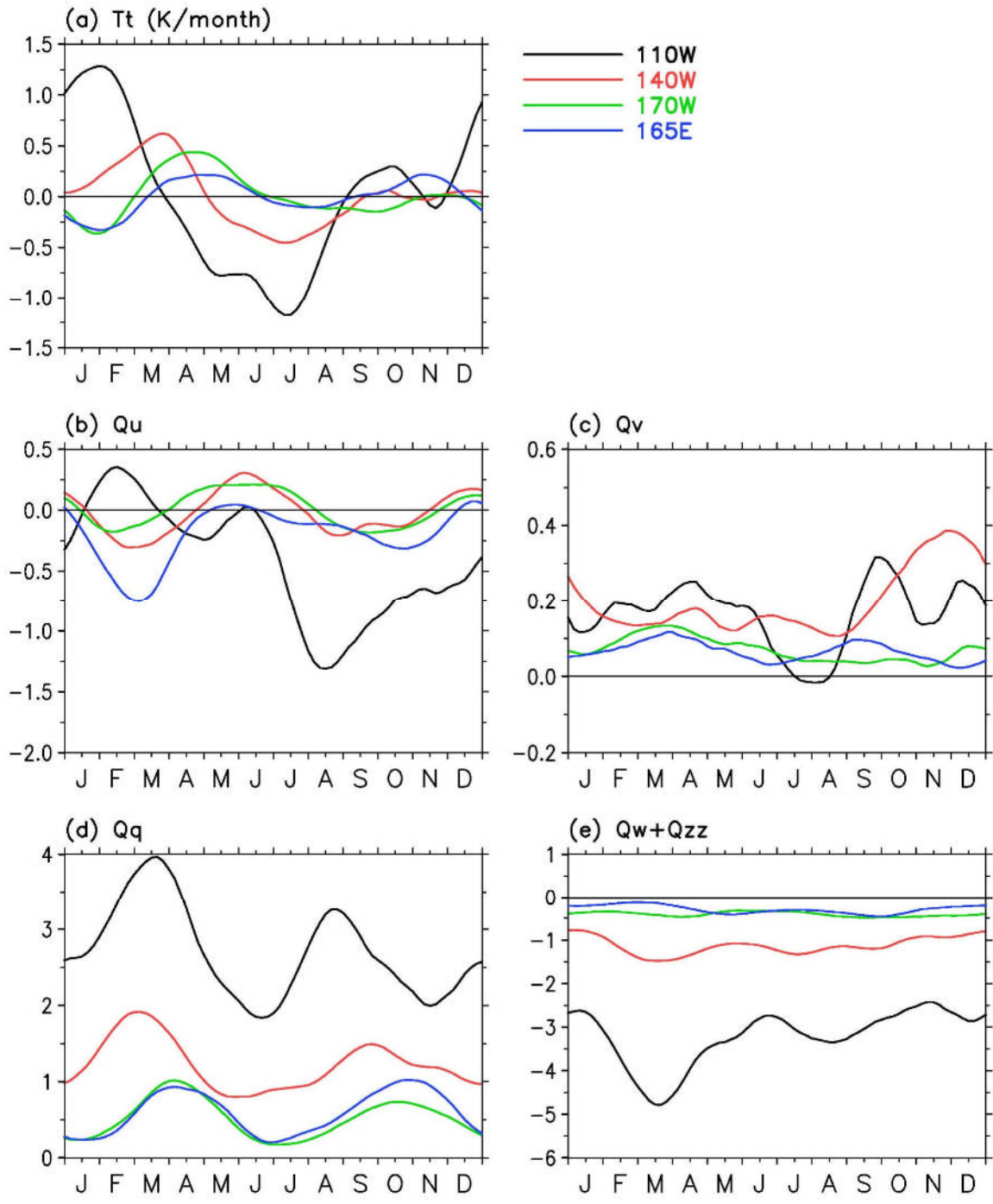


Figure 8. Unfiltered temperature budgets of the equatorial Pacific Ocean at 110°W, 140°W, 170°W, and 165°E. (a) Temperature tendency, (b) Zonal advection, (c) Meridional advection, (d) Adjusted heat flux, and (e) Entrainment and vertical diffusion. Units:  $^{\circ}\text{C mon}^{-1}$ . A 6-pentad running mean has been applied in the plots.

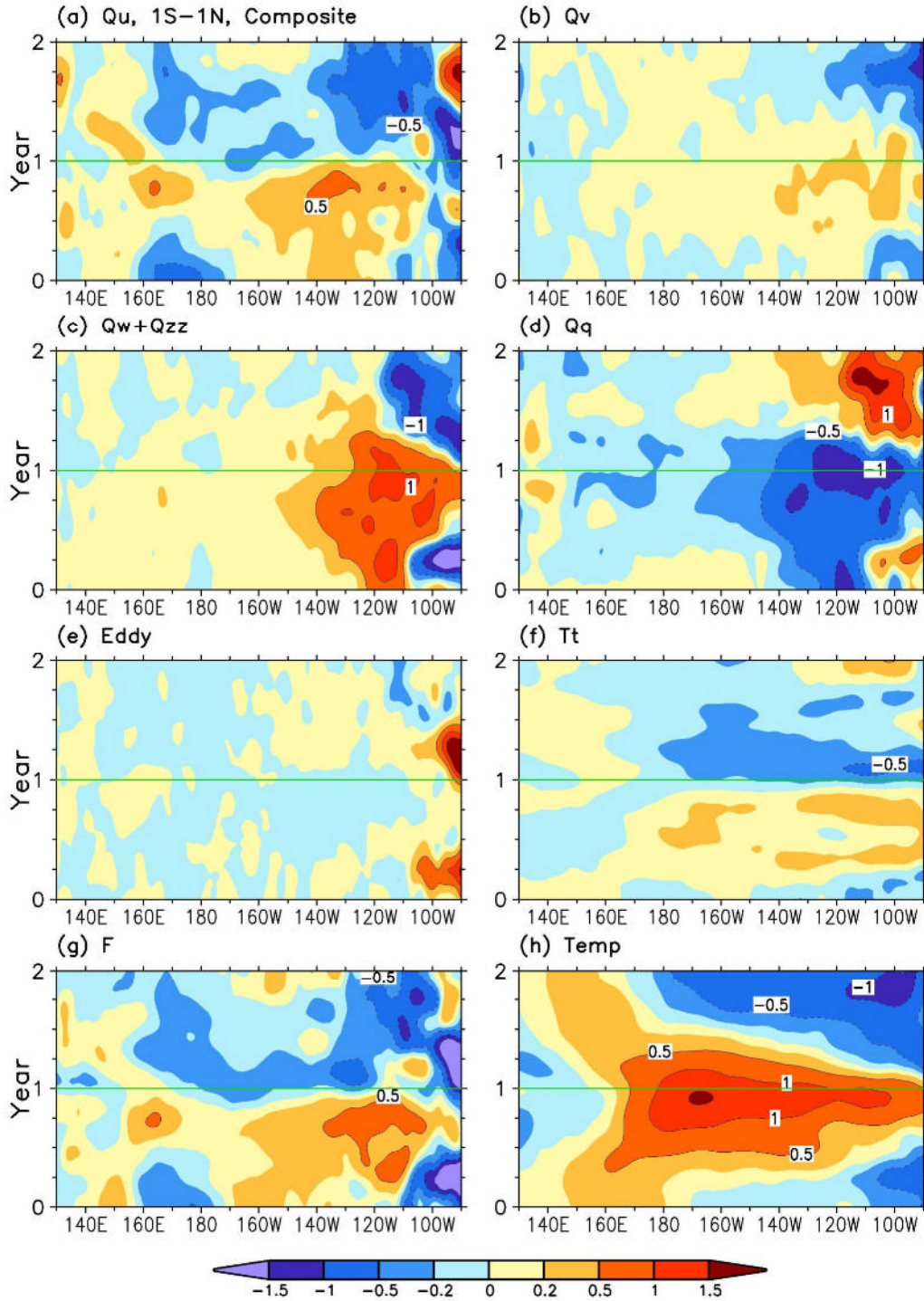


Figure 9. Low-pass filtered temperature budgets of the El Niño composite between 1°S and 1°N by (a) Zonal advection, (b) Meridional advection, (c) Entrainment and vertical diffusion, and (d) Adjusted surface heat. (e) Eddy between unfiltered and low-pass filtered budgets. (f) Unfiltered temperature tendency, (g) Unfiltered forcing in Eq (2), and (h) Unfiltered temperature. Contours are 0,  $\pm 0.2$ ,  $\pm 0.5$ ,  $\pm 1$ ,  $\pm 1.5$  and  $\pm 2$ . Units are °C mon<sup>-1</sup> in (a)-(g) and °C in (h). A 6-pentad running mean has been applied in the plots.

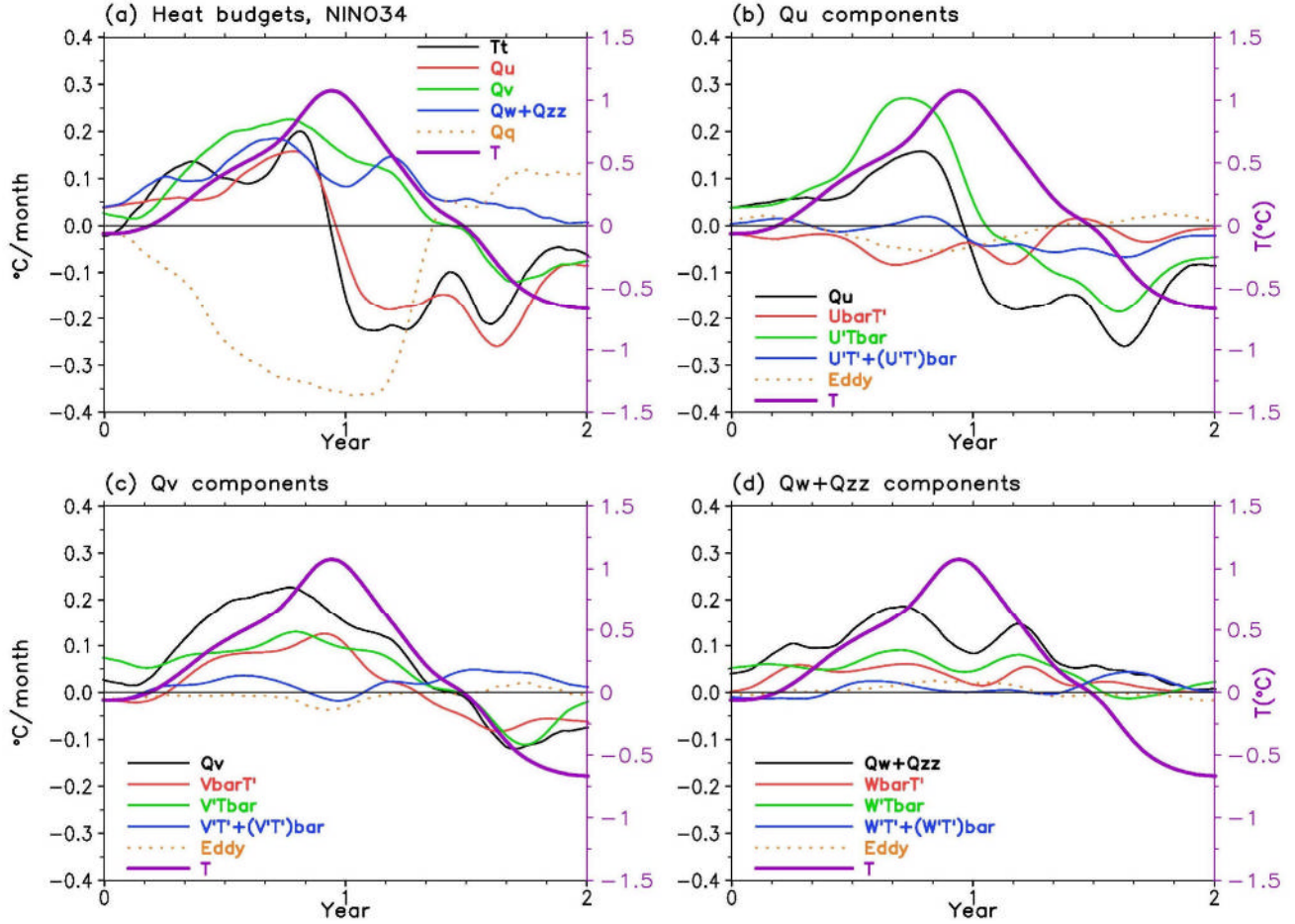


Figure 10. Temperature budget anomalies of the El Niño composite in NINO3.4 region (5°S-5°N, 120°W-170°W). (a) Unfiltered temperature budgets ( $^{\circ}\text{C mon}^{-1}$ ). Decomposition of low-pass filtered (b) Zonal advection, (c) Meridional advection, and (d) Entrainment and vertical diffusion. The unfiltered budgets in (a) are replotted in (b)-(d). Temperature anomalies are plotted in the scale of the right axis. Decomposed climatology and associated anomaly are noted as bar and prime, for example,  $U\bar{a}rT' = \bar{u} \cdot T'_x$ . The “Eddy” in (b)-(d) represents the difference between unfiltered budget anomaly in (a) and low-pass filtered budget anomaly.

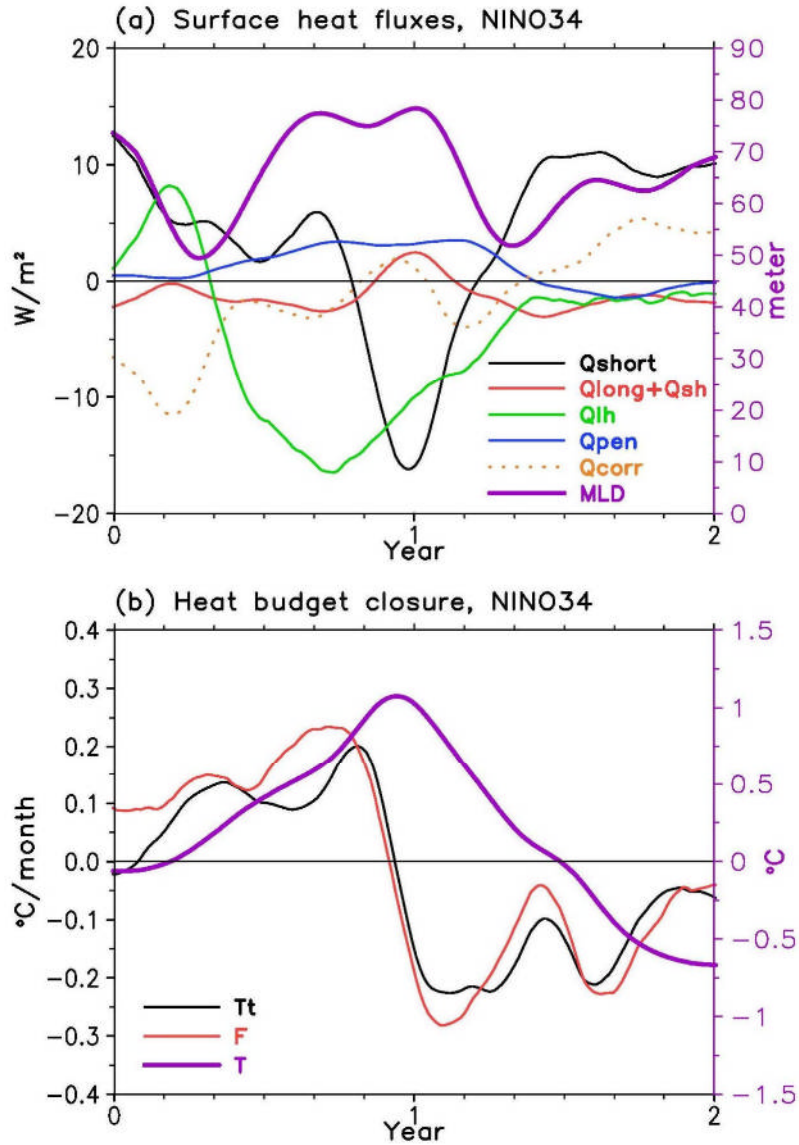


Figure 11. (a) Components of surface heat flux anomalies (left axis) and MLD (right axis) of the El Niño composite in NINO3.4 region ( $5^{\circ}S-5^{\circ}N$ ,  $120^{\circ}W-170^{\circ}W$ ). The fluxes are positive downward except for  $Q_{pen}$  that is positive upward. (b) Mixed layer heat budget closure (left axis) and mixed layer temperature anomaly (right axis) in NINO3.4 region.

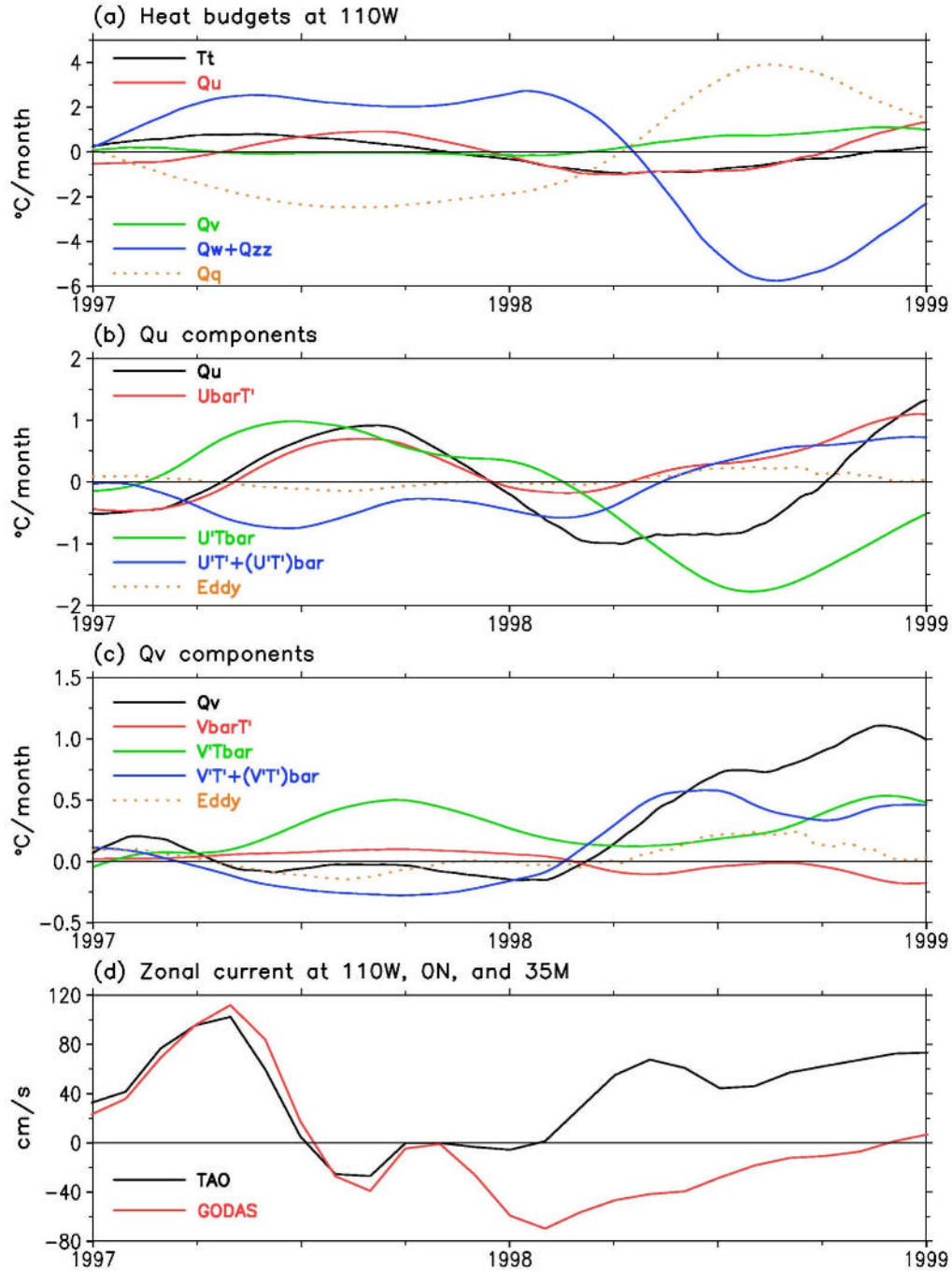


Figure 12. Temperature budget anomalies at 110°W and 0°N from 1997 to 1998. (a) Unfiltered temperature budget ( $^{\circ}\text{C mon}^{-1}$ ) at 110°W and 0°N. Decomposition of low-pass filtered (b) Zonal advection, and (c) Meridional advection. (d) Zonal current of TAO and GODAS for 1997-98 El Niño at 110°W, 0°N, and 35 m depth. A 5-month running mean and a 3-month running mean has been applied in (a)-(c), and a 3-month running mean has been applied in (d).

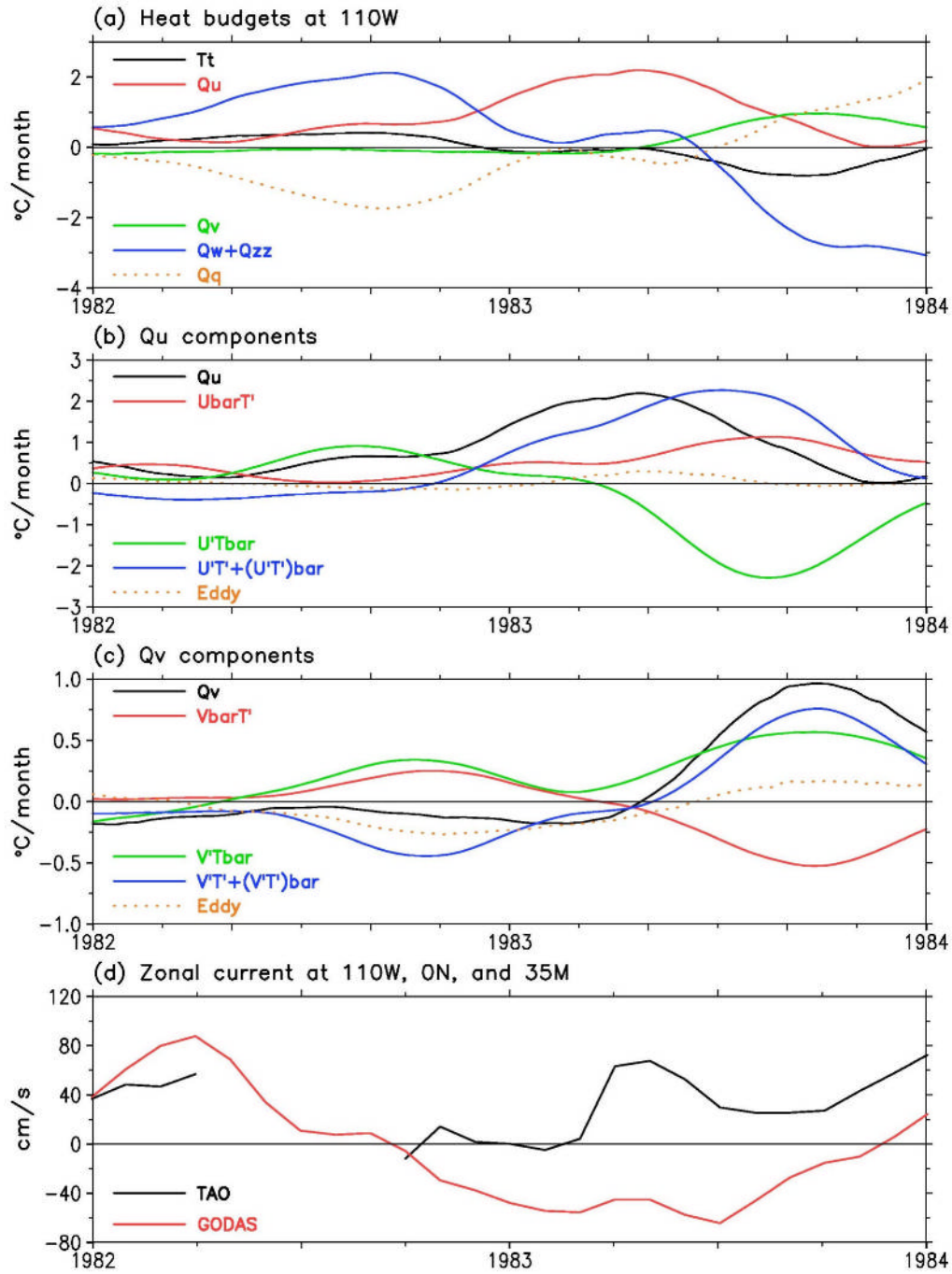


Figure 13. Same as Figure 12 except for the 1982-83 El Niño.